

# Implications of the ongoing rock uplift in NW Himalayan interiors

Saptarshi Dey<sup>1</sup>, Rasmus Thiede<sup>2</sup>, Arindam Biswas<sup>3</sup>, Naveen Chauhan<sup>4</sup>, Pritha Chakravarti<sup>1</sup>, and Vikrant Jain<sup>1</sup>

<sup>1</sup>*Earth Science Discipline, IIT Gandhinagar, Gandhinagar-382355, India.*

<sup>2</sup>*Institute of Geosciences, Christian Albrechts University of Kiel, Kiel-24118, Germany.*

<sup>3</sup>*Department of Applied Geology, IIT-ISM Dhanbad, Jharkhand-826004, India.*

<sup>4</sup>*Atomic Molecular and Optical Physics Division, Physical Research Laboratory, Ahmedabad.*

Corresponding author

Saptarshi Dey

[saptarshi.dey@iitgn.ac.in](mailto:saptarshi.dey@iitgn.ac.in)

## Abstract

The Lesser Himalayan ~~duplex~~ exposed in the Kishtwar Window (KW) of the Kashmir Himalaya exhibits rapid rock uplift and exhumation (~3 mm/yr) at least since the Late Miocene. However, it has remained unclear if it is still actively-deforming. Here, we combine new field observations, morphometric and structural analyses with dating of geomorphic markers to discuss the spatial pattern of deformation across the window. We found two steep stream segments, one at the core and the other along the western margin of the KW, which strongly suggest ongoing differential uplift and may possibly be linked either to crustal ramps on the MHT or active surface-breaking faults. ~~Longitudinal fluvial profiles document gradients changes across the entire length of the window, and high gradient changes in the core of the window.~~

22 High bedrock incision rates ( $> 3$  mm/yr) on Holocene/Pleistocene timescales are deduced from  
23 dated strath terraces along deeply-incised Chenab River valley ~~lying above the potential ramp~~  
24 ~~along the western margin of the KW~~. In contrast, farther downstream on the hanging wall of the  
25 MCT, fluvial bedrock incision rates are lower ( $< 0.8$  mm/yr) and are in the range of long-term  
26 exhumation rates. Bedrock incision rates largely correlate with previously-published  
27 thermochronologic data. ~~The obtained results can be partially explained by existence of multiple~~  
28 ~~crustal ramps which could result into differential uplift due to translation on the basal~~  
29 ~~decollement. Or, similar rock uplift can also be caused by out-of-sequence faulting at the core~~  
30 ~~and along the western margin of the window~~. In summary, our study highlights a structural and  
31 tectonic control on landscape evolution over millennial timescales.

## 32 **Keywords**

33 Steepness index; knickzone, rock strength; bedrock incision; Main Himalayan Thrust.

34

## 35 **1. Introduction**

36

37 Protracted convergence between the Indian and the Eurasian plate resulted into the  
38 growth and evolution of the Himalayan orogen and temporal in-sequence formation of the  
39 Southern Tibetan Detachment System (STDS), the Main Central Thrust (MCT), the Main  
40 Boundary Thrust (MBT) and the Himalayan Frontal Thrust (HFT) towards the south (e.g., Yin  
41 and Harrison, 2000; DiPietro and Pogue, 2004) (Supplementary Fig.B1). HFT defines the  
42 southern termination of the Himalayan orogenic wedge and separates the orogen from the  
43 undeformed foreland basin known as the Indo-Gangetic Plains. Seismic reflection profiles reveal

44 that all these fault-zones emerge from a low-angle basal decollement, the Main Himalayan  
45 Thrust (MHT) forming the base of the Himalayan orogenic wedge (e.g., Ni and Barazangi, 1984;  
46 Nabelek et al., 2009; Avouac et al., 2016), established in the late Miocene (Vannay et al., 2004).  
47 Existence of MHT has further been elaborated in Himalayan cross-sections (e.g., Powers et al.,  
48 1998; Decelles et al., 2001; Webb et al., 2011; Gavillot et al., 2018).

49 Lave and Avouac (2000) studied the late Pleistocene-Holocene shortening history of the  
50 Central Nepal Himalaya where they showed the Holocene shortening is accommodated only  
51 across the HFT. However, a large body of literature in the eastern, central and western Himalaya  
52 favored that majority of the late Pleistocene-Holocene shortening is rather partitioned throughout  
53 the Sub-Himalayan domain (morphotectonic segment in between the MBT and the MFT) and not  
54 solely accommodated by the HFT (e.g., Wesnousky et al., 1999; Burgess et al., 2012; Thakur et  
55 al., 2014; Mukherjee, 2015; Vassalo et al., 2015; Dey et al., 2016; Dey et al., 2018). The  
56 statement above implies that the northerly thrusts, i.e., the MBT and the brittle faults exposed in  
57 the vicinity of the southern margin of the Higher Himalaya, are considered inactive over  
58 millennial timescales. However, in recent years, several studies which focused on the low-  
59 Temperature thermochronologic data and thermal modeling of the interiors of the NW Himalaya  
60 have raised questions on the statement above. The recent studies suggested that 1-3 mm/yr out of  
61 the total Quaternary shortening has been accommodated in the north of the MBT as out-of-  
62 sequence deformation (Thiede et al., 2004; Deeken et al., 2011; Thiede et al., 2017) or in form of  
63 growth of the Lesser Himalayan Duplex (Gavillot et al., 2018) (Supplementary Fig. B2). For  
64 faults within the hinterland of the Central Himalaya, the out-of-sequence deformation has been  
65 explained by two end-member models. One of them favored the reactivation of the MCT (Wobus  
66 et al., 2003), while the other tried to explain all changes along the southern margin of the Higher

67 Himalaya driven by enhanced rock uplift over a major ramp on the MHT (Bollinger et al., 2006;  
68 Herman et al., 2010; Robert et al., 2009). Landscape evolution models, structural analysis and  
69 thermochronologic data from the interior of the Himalaya favor that the Lesser Himalaya has  
70 formed a duplex at the base of the southern Himalayan front by sustained internal deformation  
71 since late Miocene (Decelles et al., 2001; Mitra et al., 2010; Robinson and Martin, 2014; Gavillot  
72 et al., 2016). The growth of the duplex resulted into the uplift of the Higher Himalaya forming  
73 the major orographic barrier of the orogen. The Kishtwar Window (KW) in the NW Himalaya  
74 represents the northwestern termination of the Lesser Himalayan Duplex (LHD). While most of  
75 the published cross-sections of the Himalayan orogen today recognize the duplex structures  
76 within the Lesser Himalaya (Webb et al., 2011; Mitra et al., 2010; DeCelles et al., 2001; Gavillot  
77 et al., 2018), little or no data are available on how the deformation is spatially as well as  
78 temporally distributed and most importantly, whether a duplex is active over millennial  
79 timescales.

80         The low-temperature thermochron study by Kumar et al., (1995) portrayed the first  
81 orogen-perpendicular sampling traverse extending from the Kishtwar tectonic Window over the  
82 Zaskar Range. More recent studies link the evolution of the KW to the growth of the Lesser  
83 Himalayan Duplex structure (Gavillot et al., 2018), surrounded by the Miocene MCT shear zone  
84 along the base of the High Himalayan Crystalline, locally named as the Kishtwar Thrust (KT)  
85 (Ul Haq et al., 2019). Thermochronological constraints suggest higher rates of exhumation  
86 within the window (3.2-3.6 mm/yr) with respect to the surroundings (~0.2 mm/yr) (Gavillot et  
87 al., 2018), corroborating well with similar thermochron-based findings from the of the Kullu-  
88 Rampur window along the Beas (Stübner et al., 2018) and Sutlej valley (Jain et al., 2000;  
89 Vannay et al., 2004; Thiede et al., 2004) over the Quaternary timescale. No evidence exists

90 whether the hinterland of the Kashmir Himalaya is tectonically-active over intermediate  
91 timescales. Therefore, to understand the  $10^3$ - $10^4$ -year timescale neotectonic evolution, we  
92 combined geological field evidences, chronologically-constrained geomorphic markers and  
93 morphometric analysis of potential study areas, such as the KW. The detailed structural  
94 information of the window and the surroundings, previously-published thermochron data,  
95 accessibility, well-preserved sediment archive, and recognizable geomorphic markers across the  
96 Kishtwar Window makes it a potent location for our study.

97 In this study, we focus on the following long-standing questions on Himalayan  
98 neotectonic evolution, which are-

99 1. Is there any ongoing neotectonic deformation in the interiors of the Kashmir  
100 Himalaya?

101 2. Can we determine sub-surface structural variations and existence of surface-breaking  
102 faults by analyzing terrain morphology?

103 3. Can we obtain new constraints on deformation over geomorphic timescales? Do  
104 millennial-scale fluvial incision rates support long-term exhumation rates?

105 To address these questions, we adopted a combination of methods such as morphometric  
106 analysis using high-resolution digital elevation models, field observation on rock type, structural  
107 variations as well as rock strength data and, analysis of satellite images to assess the spatial  
108 distribution of the late Quaternary deformation of the KW and surroundings (Fig.1). We aimed to  
109 evaluate the role of active tectonics and geometric variations in the basal decollement in shaping  
110 the topography (Fig.1). We used basinwide steepness indices and specific stream power as a  
111 proxy of fluvial incision. And, lastly but most importantly, we calculated the fluvial bedrock

112 incision rates by using depositional ages of aggraded sediments along Chenab River. In this  
113 study, we show that the regional distribution of topographic growth is concentrated in the core of  
114 the window and along the western margin of the window. Our new estimates on the bedrock  
115 incision rate agree with Quaternary exhumation rates from the KW, which could mean consistent  
116 active growth of the Kishtwar Window over million-year to millennial timescales. Although the  
117 observed topographic and morphometric pattern indicate a structural/tectonic control on  
118 topographic evolution, with the available data we are not able to resolve whether it is caused by  
119 passive translation on the MHT or by active surface-breaking faulting within the duplex.

120

## 121 **2. Geological background**

122 Regionally balanced cross-sections (DiPietro and Pogue, 2004; Searle et al., 2007;  
123 Gavillot et al., 2018) suggest that the Himalayan wedge is bounded at the base by décollement,  
124 named the MHT and all regionally-extensive surface-breaking thrust systems are rooted to it.  
125 The orogenic growth of the Himalaya resulted into an overall in-sequence development of the  
126 orogen-scale fault systems which broadly define the morphotectonic sectors of the orogen (Fig.  
127 1b). Notable among those sectors, the Higher Himalaya is bordered by the MCT in the south and  
128 is comprised of high-grade metasediments, Higher Himalayan Crystalline Sequence (HHCS) and  
129 Ordovician granite intrusives (Fuchs, 1981; Steck, 2003; DiPietro and Pogue, 2004; Gavillot et  
130 al., 2018). The Low-grade metasediments (quartzites, phyllites, schists, slates) of the Proterozoic  
131 Lesser Himalayan sequence are exposed between the MCT in the north and MBT in the south.  
132 The Lesser Himalayan domain is narrow (4-15 km) in the NW Himalaya except where it is  
133 exposed in the form of tectonic windows (Kishtwar window, Kullu-Rampur window etc.) in the  
134 western Himalaya (Steck, 2003). The Sub-Himalayan fold-and-thrust belt lying to the south of

135 the MBT is tectonically the most active sector since the late Quaternary (Gavillot, 2014; Vassallo  
136 et al., 2015; Gavillot et al., 2018).

137         Near the southwest corner of our study area, Proterozoic low-grade Lesser Himalayan  
138 metasediments are thrust over the Tertiary Sub-Himalayan sediments along the MBT (Wadia,  
139 1934; Thakur, 1992). Near the Chenab region in the Kashmir Himalaya, Apatite U-Th/He ages  
140 suggest that cooling and exhumation related to faulting along the MBT thrust sheet initiated  
141 before  $\sim 5 \pm 3$  Myr (Gavillot et al., 2018). Geomorphic data obtained across the MBT in Kashmir  
142 Himalaya suggest that MBT has not been reactivated for the last 14-17 kyr (Vassallo et al.,  
143 2015). In the Kashmir Himalaya, the Lesser Himalayan sequence (LHS) exposed between the  
144 MBT and the MCT is characterized by a  $< 10$  km-wide zone of sheared schists, slates, quartzites,  
145 phyllites and Proterozoic intrusive granite bodies (Bhatia and Bhatia, 1973; Thakur, 1992; Steck,  
146 2003). The LHS is bounded by the MCT shear zone in the hanging wall. The MCT hanging wall  
147 forms highly deformed nappe exposing lower and higher Haimantas, which are related to the  
148 Higher Himalayan Crystalline Sequence (HHCS) (Bhatia and Bhatia, 1973; Thakur, 1992; Yin  
149 and Harrison, 2000; Searle et al., 2007; Gavillot et al., 2018). Nearly 40 km NE of the frontal  
150 MCT shear zone, MCT fault zone is re-exposed as a klippe in the vicinity of KW is called the  
151 Kishtwar Thrust (KT) (Ul Haq et al., 2019) (fig. 1). Within the KW, Lesser Himalayan  
152 quartzites, low-grade mica schists and phyllites along with the granite intrusives are exposed  
153 (Fuchs, 1975; Steck, 2003; DiPietro and Pogue, 2004; Yin, 2006; Gavillot et al., 2018).

## 154                                   **2.1. Structural architecture of the Kishtwar Window**

155         The sub-surface structural formation beneath the KW is not well-constrained. A recent  
156 study by Gavillot et al., (2018) proposes that the KW exposes a stack of LHS nappes in form of  
157 the commonly-known Lesser Himalayan Duplex (LH duplex), characteristic of the central

158 Himalaya (Decelles et al., 2001). They also propose the existence of two mid-crustal ramps  
159 beneath the KW, viz., MCR-1 and MCR-2 (fig. 1b). Based on thermochronological constraints  
160 from Kumar et al., (1995), Gavillot et al. (2018) proposed that the core of the window is  
161 exhumed with rates 3.2-3.6 mm/yr during the Quaternary, at a higher rate when compared to the  
162 surroundings (~0.2-0.4 mm/yr). However, earlier studies by Fuchs (1975) and Frank et al.,  
163 (1995) provide different insights to the formation of the KW. Fuchs (1975) proposed the  
164 existence of two nappes- a. the Chail Nappe and b. the Lower Crystalline Nappe. The Lower  
165 Crystalline nappe is partially or completely included in the MCT (KT) shear zone and the Chail  
166 nappe encompasses the core of the window (Stephenson et al., 2000). According to these studies,  
167 the Chail nappe has been internally deformed by crustal buckling, tight isoclinal folding causing  
168 repetition and thickening of the LH crust.

169         The Higher Himalayan sequence dips steeply away from the duplex (~65° towards west)  
170 (Fig.1, 2a). The frontal horses of the LH duplex expose internally-folded greenschist facies  
171 rocks. Although at the western margin of the duplex, the quartzites stand sub-vertically (Fig.2c),  
172 the general dip amount reduces as we move from west to east for the next ~10-15 km up to the  
173 core of the KW. Near the core of the KW, we observed highly-deformed (folded and multiply-  
174 fractured) quartzite at the core of the KW (Fig.2d, 2e). We also observed deformed quartz veins  
175 of at least two generations, as well as macroscopic white mica. Here, the Chenab River is also  
176 very steep and narrow; the rock units are also steeply-dipping towards the east (~55-65°) and are  
177 nearly isoclinal and strongly deformed at places (Fig.2f). Towards the eastern edge of the  
178 window, however, the quartzites dip much gently towards the east (~20-30°) (Fig.1b), and much  
179 lesser folding and faulting have been recognized in the field (Fig.2g).

## 180                   **2.2.Valley morphology**

181 The broad, 'U-shaped' valley profile near the town of Padder at the eastern margin of the  
182 KW is in contrast with the interior of the window (Fig.3a). At the core of the KW, the Chenab  
183 River maintains a narrow channel width and a steep gradient (Fig.3b). The E-W traverse of the  
184 Chenab River through the KW is devoid of any significant sediment storage. However, along the  
185 N-S traverse parallel to the western margin of the KW, beneath the Kishtwar surface, ~150-170m  
186 thick sedimentary deposits are transiently-stored over the steeply-dipping Higher Himalayan  
187 bedrock (Fig.3c). The height of the Kishtwar surface from the Chenab River is ~450m, which  
188 means ~280m of bedrock incision by the River since the formation of the Kishtwar surface.  
189 Along the N-S traverse of the River, epigenetic gorges are formed as a result of the damming of  
190 paleo-channel by the hillslope debris flow, followed by the establishment of a newer channel  
191 path (Ouimet et al., 2008; Kothyari and Juyal, 2013). One example of such epigenetic gorge  
192 formation near the town of Drabshalla is shown in Fig.3d. Downstream from the town of  
193 Drabshalla, the River maintains narrow channel width (< 25 m) and flows through a gorge  
194 having sub-vertical valley-walls (Fig.3e). The tributaries originating from the Higher Himalayan  
195 domain form one major knickpoint close to the confluence with the trunk stream (Fig.3f). We  
196 have identified at least three strath surface levels above the present-day river channel, viz., T1  
197 ( $280\pm 5$  m), T2 (170-175 m) and T3 ( $\sim 120\pm 5$  m), respectively (Fig.3g). The first study on  
198 sediment aggradation in the middle Chenab valley (transect from Kishtwar to Doda town) was  
199 published by Norin (1926). He argued the sediment aggradation in and around the Kishtwar town  
200 is largely contributed by fluvio-glacial sediments and the U-shaped valley morphology is a  
201 marker of past glacial occupancy. In general, we agree with the findings of Norin (1926) and UI  
202 Haq et al., (2019) as we observe ~100m thick late Pleistocene fluvio-glacial sediment cover  
203 unconformably overlying the Higher Himalayan bedrock, most likely to be paleo-strath surface

204 (Fig.4b). At the same time, we do not agree with the interpretation of surface-breaking faults  
205 near Kishtwar town by Ul Haq et al. (2019). We inspected the proposed fault locations in detail  
206 and didn't observe any evidence of large-scale fault movement, including offset, broken and  
207 rotated clasts, fault gouges etc. on the proposed fault planes. There is only one evidence of a  
208 deformed sand layer which shows tilting and offset (<1 m). Therefore, we may conclude that we  
209 found no strong evidence of any large-scale surface-breaking faults. The fluvio-glacial sediments  
210 included alternate layers of pebble conglomerate and coarse-medium sand (Fig.4c). The pebbles  
211 are moderately rounded and polished suggesting significant fluvial transport. Our field  
212 observations suggest that the fluvio-glacial sediments have been succeeded by a significant  
213 volume of hillslope debris flow and paleo-landslide deposit (Fig.4c). The thickness of the debris-  
214 flow deposits is variable. The hillslope debris units and landslide deposits contain mostly  
215 massive, highly-angular, poorly-sorted quartzite clasts from the steep western margin of the KW.  
216 The hillslope debris units also contain a few fine-grain sediment layers trapped in between two  
217 coarse-grained debris layers (Fig.4e). The town of Kishtwar is situated on this debris flow  
218 deposit.

219

### 220 **3. Methods of morphometric analysis and field data collection**

221

#### 222 **3.1.Morphometry**

223 For conducting the morphometric analysis, we have used 12.5m ALOS-PALSAR DEM  
224 data (high resolution terrain-corrected) (Fig.5a). This DEM data has lesser issues with artifacts  
225 and noises than 30m SRTM data, which fails to capture the drainage network properly in areas  
226 populated by narrow channel gorges. Topographic relief has been calculated using a 4km moving

227 window (Fig.5b) and the rainfall distribution pattern has been adapted from 12-year averaged  
228 annual rainfall data (TRMM data: Bookhagen and Burbank, 2006) (Fig.5c).

### 229 **3.1.1. Drainage network extraction**

230 The drainage network and the longitudinal stream profiles were extracted using the  
231 Topographic Analysis Kit toolbox (Forte and Whipple, 2019). An equivalent of 10-pixel  
232 smoothing of the raw DEM data has been applied to remove noises from the DEM. The  
233 longitudinal stream profile of the Chenab trunk stream was processed with the Topotoolbox  
234 ‘Knickpointfinder’ tool (Schwanghart and Scherler, 2014). Several jumps/ kinks in the  
235 longitudinal profile are seen and those are marked as knickpoints (Fig.6). A 30m tolerance  
236 threshold was applied to extract only the major knickpoints.

### 237 **3.1.2. Basinwide normalized steepness indices**

238 Global observations across a broad spectrum of tectonic and climatic regimes have  
239 revealed a power-law scaling between the local river gradient and upstream contributing area:

$$240 \quad S = k_s \cdot A^{-\theta} \quad (1)$$

241 where S is the stream gradient (m/m),  $k_s$  is the steepness index ( $m^{2\theta}$ ), A is the upstream  
242 drainage area ( $m^2$ ), and  $\theta$  is the concavity index (Flint, 1974; Whipple and Tucker, 1999).  
243 Normalized steepness-index values ( $k_{sn}$ ) are steepness indices calculated using a reference  
244 concavity value ( $\theta_{ref}$ ), which is useful to compare steepness-indices of different river systems  
245 (Wobus et al., 2006). We extracted the  $k_{sn}$  values in the study area using the ArcGIS and  
246 MATLAB-supported Topographic Analysis Toolkit (Forte and Whipple, 2019) following the  
247 procedure of Wobus et al. (2006). We performed an automated  $k_{sn}$  extraction using a critical area  
248 of  $10^6 m^2$  for assigning the channel head, a smoothing window of 500 m, a  $\theta_{ref}$  of 0.45, and an  
249 auto- $k_{sn}$  window of 250 m for calculating  $k_{sn}$  values. The slope-breaks, known as the knickpoints

250 (sometimes referred to as knickzones if it is manifested by a series of rapids instead of a single  
251 sharp break in profile), were allocated by comparing the change of slope along the distance-  
252 elevation plot (Fig.6, 7a). Threshold 'dz' value (projected stream offset across a knickpoint) for  
253 this study is 30m. Basinwide mean  $k_{sn}$  values are plotted using a 1000 km<sup>2</sup> threshold catchment  
254 area (Fig. 5d).

255 Identification of the knickpoints/ knickzones and their relationship with the rock-types as  
256 well as with existing structures are necessary to understand the causal mechanism of the  
257 respective knickpoints/ knickzones. Knickpoints/(zones) can be generated by lithological,  
258 tectonic and structural control. Lithological knickpoints are stationary and anchored at the  
259 transition from the soft-to-hard substrate. The tectonic knickpoints originate at the active tectonic  
260 boundary and migrate upstream with time. Structural variations, such as thrust fault ramp-flat  
261 geometry may cause a quasistatic knickpoint at the transition of the flat-to-ramp of the fault. In  
262 such cases, the ramp segment is characterized by higher steepness than the flat segment and at  
263 times the ramp may be characterized by a sequence of rapids, forming a wide knickzone, instead  
264 of a single knickpoint.

### 265 **3.1.3. Channel Width**

266 Channel width is a parameter of assessment of lateral erosion/incision through bedrocks  
267 of equivalent strength (Turowski, 2009). The channel width of the Chenab trunk stream from just  
268 downstream of the MBT up to the eastern margin of the KW was derived by manual selection  
269 and digitization of the channel banks using the Google Earth Digital Globe imagery  
270 (<http://www.digitalglobe.com/>) of minimum 3.2 m spatial resolution. We used the shortest  
271 distance between the two banks as the channel width. We rejected areas having unparallel  
272 channel-banks as that would bias the result. We used a 50 m step between two consecutive points

273 for channel width determination. Twenty point-averaged channel width data along with elevation  
274 of the riverbed is shown in Fig.7b.

#### 275 **3.1.4. Specific stream power (SSP) calculation**

276 Specific stream power has often been used as a proxy of fluvial incision or differential  
277 uplift along the channel (Royden and Perron, 2013; Whipple and Tucker, 1999). Areas of higher  
278 uplift/incision are characterized by transient increase in the specific stream power. Channel slope  
279 and channel width data were used to analyse the corresponding changes in the specific stream  
280 power (SSP) from upstream of the gorge area to the gorge reaches (Bagnold, 1966). The SSP ( $\omega$ )  
281 was estimated using the following equation –

$$282 \quad \omega = \gamma \cdot Q \cdot s / w \quad (\text{Eq. 1})$$

283 Where,  $\gamma$  - unit weight of water, Q – water discharge, s – energy slope considered  
284 equivalent to the channel slope; w – channel width. SSP data from selected stretches are shown  
285 in Table 1. Channel width has been adapted from method described in section 3.1.3. We assumed  
286 a uniform discharge throughout the study area, as the TRMM data show insignificant variations  
287 in mean annual rainfall (Bookhagen and Burbank, 2006) (Fig. 5c, 5e). We also assume a runoff  
288 ratio of 1 as we don't have any independent measure or supportive data of runoff vs. water  
289 percolation through the bedrock and sediment archive.

290

### 291 **3.2. Field data collection**

#### 292 **3.2.1. Structural data**

293 We measured the strike and dip of the foliations and bedding planes of the Lesser and  
294 Higher Himalayan rocks using the Freiberg clinometer compass. At least five measurements are

295 taken at every location and the average of them has been reported in Fig. 8a. Field photos in the  
296 Fig.2 support observed variations in the structural styles.

### 297 **3.2.2. Rock strength data**

298 Recording rock strength data in the field is important to understand the role of variable  
299 rock-type and rock-strength in changes in morphology. It provides us important insights on the  
300 genesis of knickpoints whether they are lithologically-controlled or not. It also helps to  
301 understand the variations in channel steepness across rocks of similar lithological strength. We  
302 systematically measured the rock strength of the main geologic units using a hand-held rebound  
303 hammer. Repeated measurements (8-10 measurements at each of the 75 locations throughout the  
304 study area) were conducted to measure the variability of rock-strength within the main lithologic  
305 units (Fig. 7e). All the measurements were taken perpendicular to the bedding/ foliation plane,  
306 and, no measurements are from wet surfaces or surfaces showing fractures. Each reading was  
307 taken at least 0.5m apart from the previous one. To our benefit, most of the road-cut sections had  
308 bedrock-exposures. Except restricted locations, e.g., dam-sites and military bases and outposts,  
309 we were able to cover rest of the study area. To add to this, data taken from Higher Himalayan  
310 intrusives close to the western margin of the KT are positively-biased as it represents readings  
311 only from the leucosomatic layers. Our data from individual sites are smaller in number than  
312 what is preferred for checking the statistical robustness of Schmidt hammer data (Niedzielski et  
313 al., 2009). Therefore, we combined the data from all sites representing similar lithology and  
314 portrayed the mean  $\pm$ standard deviation for the same. Field data on rock strength measurement  
315 has been provided in Supplementary Table C1.

### 316 **3.3.Luminescence dating of transiently-stored sediments in and around** 317 **Kishtwar**

318 Luminescence dating of Quaternary sediments is a globally accepted method for  
319 constraining the timing of deposition of sediments across different depositional environments,  
320 viz., Aeolian (Juyal et al., 2010), fluvial (Olley et al., 1998; Cunningham and Wallinga, 2012)  
321 and glacial origin (Owen et al., 2002; Pant et al., 2006). In this study, we used luminescence  
322 dating techniques to constrain depositional ages of several fluvioglacial and fluvial sand layers  
323 exposed near the western margin of the KW and further downstream. Although there exists a few  
324 persistent problems in luminescence dating of the Himalayan sediments (including poor  
325 sensitivity of quartz and numerous cases of heterogeneous bleaching of the luminescence signal),  
326 studies over the past couple of decades have also provided a good control on Himalayan  
327 sedimentary chronology by using luminescence dating with quartz (Optically stimulated  
328 luminescence, OSL) and feldspar (Infra-red stimulated luminescence, IRSL).

329 Samples K-07, K-08 and K-09 were collected from the medium-coarse sand beds of  
330 fluvioglacial origin and have been dated with IRSL technique (Preusser, 2003). Standard IR-  
331 protocol was used because the OSL signal was saturated and postIR-IR was showing instances of  
332 heterogeneous bleaching. Samples K-02 and K-11 were taken from the fine sand-silt layers lying  
333 above the debris-flow deposits and have been treated for OSL dating using double-SAR (single  
334 aliquot regenerative) protocol (Roberts, 2007). Double-SAR protocol was used to surpass the  
335 luminescence signal from tiny feldspar inclusions within individual quartz grains. Samples K-16  
336 and K-17 taken above the T3 strath level, as well as the sample K-18, taken from above the T1  
337 strath level were treated/ measured following the OSL double-SAR protocol. Samples K-01 and  
338 K-06 taken above the bedrock strath near the town of Doda were also measured following OSL  
339 double-SAR protocol. The aliquots were considered for equivalent dose (ED) estimation only if:  
340 (i) recycling ratio was within  $1 \pm 0.1$ , (ii) ED error was less than 20%, (iii) test dose error was less

341 than 10%, and (iv) recuperation was below 5% of the natural. Fading correction of the IRSL  
342 samples K-07 and K-09 were done using conventional fading correction method (Huntley and  
343 Lamothe, 2001). For samples showing over-dispersion (OD)  $\leq 20\%$ , central age model (CAM)  
344 has been used for estimation of equivalent dose (De) (Bailey and Arnold, 2006) instead of  
345 RMM-based De estimation as prescribed by Chauhan and Singhvi, (2011), useful for samples  
346 having higher over dispersion (Table 2). For samples K-16 and K-17 having high OD value,  
347 minimum age model (MAM) has been used. Details of sample preparation are provided in  
348 supplement.

349 The dose rate was estimated using online software DRAC (Durcan et al., 2015) from the data of  
350 Uranium (U), Thorium (Th) and Potassium (K) measured using ICP-MS and XRF (Table 42) in  
351 IISER Kolkata. The estimation of moisture content was done by using the fractional difference  
352 of saturated vs. unsaturated sample weight (Table 42).

## 353 **4. Results**

354

### 355 *4.1. Field observations and measurements*

356 The Chenab River has deeply incised the KW (Fig. 3b and 3e). The LHS rock units  
357 exposed within the KW are mainly composed of fine-grain Quartzites and phyllites with  
358 occasional schists in between. (Steck, 2003; Gavillot et al., 2018). The Lesser Himalaya has been  
359 suggested to be an asymmetric antiformal stack with a steeper western flank (dip: 70°/west)  
360 (Fig.2c). The KW is surrounded by rock units related to the Higher Himalayan high-grade  
361 metasedimentary sequence, mainly garnet-bearing mica schists and gneisses. Higher Himalayan  
362 rocks close to the western edge of the KW form a klippe with a southwest-verging MCT at its'  
363 base. The KT, southern structural boundary of the window margin accommodating the

364 differential exhumation between window internal and surroundings, is expressed as highly  
365 deformed sub-vertical shear bands.

366 Along the traverse of the Chenab River through the KW and further downstream, two  
367 prominent stretches along the Chenab River ~20 and ~25-30 km length are characterized by  
368 steep channel gradient associated with a large number of rapids (Fig.3b). These steep segments  
369 are also characterized by a very narrow channel width (< 30m) (Fig.3b, 3e). The steepened  
370 segments define knickzone (KZ) rather than a single knickpoint (KP). The knickzones KZ1 in  
371 the trunk stream as well as in the tributaries are hosted over bedrock gorges. Although the  
372 knickzone KZ2 pass through a series of old landslides (around Kishtwar town), the rapids have  
373 all formed in bedrock channel. Therefore, neither KZ1 nor KZ2 appears to be related to  
374 damming by recent landslides or other mass movements. The eastern margin of the KW is  
375 characterized by a wide 'U-shaped' valley filled with thick sand layers and coarser fluvio-glacial  
376 sediments (Fig. 3a) where the Chenab River incises through this Late Pleistocene fill at present.

377 The rock strength data taken along the Chenab trunk stream portray large variations (R-  
378 value ranging from 28 to 62) across different morphotectonic segments (Fig.7e). Within the KW,  
379 Lesser Himalayan phyllites and schists have low R values (30-35); however, the low-strength  
380 schists and phyllites are sparsely present and therefore, they are ignored while plotting the  
381 regional rock strength values in Fig.7e. The dominant Lesser Himalayan quartzites in KW, as  
382 well as the granitic intrusives in the eastern part of the KW, shows very high R values of 55-62  
383 and 51-56 respectively (Fig. 7e). Compared to the high R values in the KW, the Higher  
384 Himalayan metasediments show low strength (R: 35-45) till the point L2KP5 (Fig. 3b).  
385 However, near the western margin of the KW, the migmatites of Higher Himalayan domain  
386 show high rock strength (R value:  $58 \pm 3$ ) (Fig.7e). The rock strength increases within the

387 Haimanta Formation (R:  $44\pm 2$ ) further downstream until it reaches the MCT shear zone at the  
388 southern boundary of the Main Himalayan orogen. The R-value in the frontal Lesser Himalaya is  
389 moderate (R:  $41\pm 2$ ).

390 The Higher Himalayan sequence dips steeply away from the duplex ( $\sim 65^\circ$  towards west)  
391 (Fig.2a, 8a). The frontal nappes of the Lesser Himalaya expose internally-folded greenschist  
392 facies rocks. Although at the western margin of the duplex, the quartzites stand sub-vertically,  
393 the general dip amount reduces as we move from west to east for the next  $\sim 10$ -15 km (Fig. 8).  
394 Near the core of the KW, we observed deformed quartz veins of at least two generations, as well  
395 as macroscopic white mica. Near the core of the window, where the river is also very steep and  
396 narrow, the rock units are also steeply-dipping towards the east ( $\sim 60$ - $65^\circ$ ) and are extremely  
397 nearly isoclinal and vigorously deformed at places (Fig.2d, 2e). Towards the eastern edge of the  
398 window, however, the quartzites dip much gently towards the east ( $\sim 25$ - $30^\circ$ ) and much lesser  
399 folding and faulting have been recognized in the field.

400 The E-W traverse of the Chenab River is completely devoid of any sediment storage.  
401 However, along the N-S traverse parallel to the western margin of the KW,  $\sim 150$ - $170$ m thick  
402 sedimentary deposits are transiently-stored over the steeply-dipping Higher Himalayan bedrock.  
403 ~~The first study on sediment aggradation in Middle Chenab valley (transect from Kishtwar to~~  
404 ~~Doda town) was published by~~ Norin (1926). ~~He~~ argued the sediment aggradation in and around  
405 the Kishtwar town is largely contributed by fluvio-glacial sediments and the U-shaped valley  
406 morphology is a marker of past glacial occupancy. We partially agree to the findings of Norin  
407 (1926) and Ul Haq et al., (2019) as we observe  $>100$ m thick fluvio-glacial sediment cover  
408 unconformably overlying the Higher Himalayan bedrock along the N-S traverse of the Chenab  
409 River. The fluvio-glacial sediments included alternate layers of pebble conglomerate and coarse-

410 medium sand. The pebbles are moderately rounded and polished suggesting significant fluvial  
411 transport. Our field observations suggest that the fluvioglacial sediments have been succeeded by  
412 a significant volume of hillslope debris. The thickness of the debris-flow deposits is variable.  
413 The hillslope debris units contain mostly coarse-grained, highly-angular, poorly-sorted quartzite  
414 clasts from the frontal horses of the Lesser Himalayan Duplex. The town of Kishtwar is situated  
415 on this debris flow deposit (Fig.9). Along the N-S traverse of the Chenab, we have observed at  
416 least two epigenetic gorges lying along the main channel (Fig. 3d). The active channel has  
417 incised the Higher Himalayan bedrock and formed strath surfaces. We have identified at least  
418 three strath surface levels above the present-day river channel, viz., T1 (280±5 m), T2 (170-175  
419 m) and T3 (~120±5 m), respectively (Fig.3g, 10a).

## 420 **4.2. Results from morphometric analysis**

### 421 *4.2.1. Steep stream segments and associated knickpoints*

422 The longitudinal stream profile along the Chenab River does not portray a typical  
423 adjusted concave-up profile across the Himalaya (Fig. 6). We observe breaks in slope and  
424 concavity at several locations within a ~150 km traverse upstream from the MBT across the KW.

425 These breaks are defined as knickpoints-. Starting from the eastern margin of the KW till the  
426 MBT in the downstream, we identified at least six (6) discrete knickpoints in the river profile  
427 (Fig. 6). Those are named KP1–KP6 according to their decreasing elevations. The upstream head  
428 of KZ1 and KZ2 are marked as KP2 and KP3, respectively (Fig. 6).~~or knickzones depending on~~  
429 ~~their type characteristics.~~ The slope breaks define the upstream reaches of the steep stream  
430 segments. The basinwide steepness indices span from ~30- >750 m<sup>0.9</sup> across the study area (Fig.  
431 5d). We assigned a threshold value of  $k_{sn} > 550$  for the steepest watersheds/ stream segments.

432 Along the traverse, the major knickpoints are ~~K1~~ KP1 (~1770m), KP2 (~1700m), ~~K2~~ KP3

433 | (~1150m) and K2-KP5 (~800m) respectively (Fig.6). Two minor knickpoints are there- KP4  
434 | (~1000m) and KP6 (~650m).

435 |         Already Nennowitz et al., (2018) had proposed a high basin-averaged  $k_{sn}$  value of  $> 300$   
436 | in the KW. Here in this study, we worked with a much-detailed DEM and stream-specific  $k_{sn}$   
437 | allocation (Fig.7d), as well as a basinwide steepness calculation. Our results corroborate with the  
438 | earlier findings, but, predict the zone of interest in greater detail. It is important to note that by  
439 | setting a higher tolerance level in the ‘knickpointfinder’ tool in Topotoolbox, we have managed  
440 | to remove the DEM artifacts from consideration (Schwanghart and Scherler, 2014).

#### 441 |         **4.2.2. Channel width and valley morphology**

442 |         The channel width of the Chenab River is on average low (30-60m) within the core of the  
443 | KW (Fig. 3b, 7b), and the low channel width continues till the Chenab River flows N-S along the  
444 | western margin of the KW. However, there are a few exceptions; upstream from the knickpoint  
445 | K1KP1 in the Padder valley (in which the town of Padder is located), the channel widens (width  
446 | ~80-100m) and the channel gradient is low (Fig. 3a). The second instance of a wider channel is  
447 | seen upstream from knickpoint K2KP3, where there is a reservoir for the Dul-Hasti dam.  
448 | Downstream from K2-KP3 within the Higher Himalaya, the channel width ranges from 50-70 m.  
449 | However, towards the lower stretches of the N-S traverse, the width is even lower (16-52m). The  
450 | river width increases to 100-200m as Chenab River takes a westward path thereafter. The ~~river~~  
451 | channel width increases beyond 300m until it leaves the crystalline rocks in the hanging wall of  
452 | the MCT and enters the Lesser Himalaya in the hanging wall of the MBT across the Baglihar  
453 | dam. Within the frontal LH, the channel width is again lowered (50-80 m).

#### 454 |         **4.2.3. Changes in specific stream power (SSP)**

455 Discharge-normalized SSP data calculated from the upstream stretches and the  
456 knickzones, KZ1 and KZ2 show major increase in SSP within the steep knickzones. The increase  
457 in SSP from upstream to the knickzones KZ1 and KZ2 are 4.44 and 5.02 times, respectively  
458 (Table 1). Such high increase in SSP is aided by steepening of channel gradient (Fig.7c) and  
459 narrowing of channel bed (Fig.7b).

### 460 **4.3. Luminescence chronology**

461 The results for the luminescence chronology experiment are listed in Table 2. Samples  
462 collected from the fluvio-glacial sediments overlain by debris flow deposit, namely as, K07, K08  
463 and K09 yield IRSL ages of  $104.5 \pm 5.9$  kyr,  $114.4 \pm 6.3$  kyr, and  $119.2 \pm 6.8$  kyr, respectively.  
464 Fading corrections done for samples K07 and K09 yield the correction factors (g%) of 0.89 and  
465 1.11 respectively. The sample K08 has not been treated for fading correction, but for easier  
466 understanding, we have assumed a constant sedimentation rate between the samples K07 and  
467 K09 and extrapolated the 'fading-corrected' age for K08. The oldest sample K09 ( $132 \pm 7$  kyr)  
468 (fading-corrected IRSL age) is succeeded by samples K08 ( $126 \pm 6$  kyr) and K07 ( $113 \pm 6$  kyr)  
469 respectively. The finer fraction of the hillslope debris overlying the fluvio-glacial deposits yield  
470 OSL ages of  $81.1 \pm 4.6$  kyr (K02) and  $85 \pm 5$  kyr (K11) (Fig.6). OSL samples taken from sparsely-  
471 preserved sediment layers above the T3 strath surface shows heterogeneous bleaching and hence  
472 we provide a minimum age of  $22.8 \pm 2.1$  kyr (sample K16) and  $20.5 \pm 1.0$  kyr (sample K17). One  
473 sample taken above T1 strath level is saturated and shows a minimum age of  $52.1 \pm 2.8$  kyr  
474 (sample K18) (Table 2). OSL samples K01 and K06 taken from sand layers sitting atop the  
475 Higher Himalayan bedrock straths near the town of Doda portray depositional ages of  $49.8 \pm 2.9$   
476 kyr and  $51.6 \pm 2.4$  kyr, respectively (Table 2).

477

## 478 5. Discussions

479

480 ~~Morphometric Analysis of morphometric~~ parameters are widely used as indicators of  
481 active tectonics and transient topography (Kirby and Whipple, 2012; Seeber and Gornitz, 1983).  
482 Many studies have used morphometry as a proxy for understanding the spatial distribution of  
483 active deformation across certain segments of the Himalayan front (Malik and Mohanty, 2007;  
484 van der Beek et al., 2016; Nennowitz et al., 2018; Kaushal et al., 2017). More importantly, some  
485 studies have integrated morphometric analysis with chronological constraints to assess the spatial  
486 and temporal variability in deformation within the Sub-Himalaya (Lave and Avouac, 2000;  
487 Thakur et al., 2014; Vassalo et al., 2015; Dey et al., 2016; Srivastava et al., 2018). All these  
488 studies have ~~demonstrated the applicability of~~~~shown that~~ morphometric indicators ~~as an can also~~  
489 ~~be used for a qualitative~~ estimate of changes in uplift rate or spatial variations of deformation  
490 ~~across different landscapes, even in the Sub-Himalayan domain where the rivers are often~~  
491 ~~alluviated due to high sediment load (Malik and Mohanty, 2007).~~ ~~Therefore, using~~  
492 ~~morphometric indices to examine some prospect areas and using their relative difference as a~~  
493 ~~proxy of relative changes in faulting and differential uplift as well as connecting these regions~~  
494 ~~with nearby regions having chronological constraints on short intermediate timescale~~  
495 ~~deformation, is a potent option, when applied carefully.~~

496 ~~Previously-published The KW exhibits~~ younger Apatite fission-track cooling ages (~ 2-3  
497 Myr) ~~as compared to the surrounding Higher Himalaya, which~~ have been interpreted as the result  
498 of rapid exhumation of the LH duplex over  $10^6$ -year timescale (Gavillot et al., 2018). However,  
499 ~~how and where the we lack any measurements of~~ deformation ~~is accommodated~~ across the KW  
500 over the  $10^3$ - $10^5$ -year timescale ~~is unknown.~~ ~~With the existing AFT data and assuming that no~~

501 ~~major changes of the deformation regime have taken place since the Quaternary, we may well~~  
502 ~~use it for calibration of morphometric proxies and interpolate these estimates to regions, where~~  
503 ~~no thermochronological constraint exists. In this section, we discuss the obtained morphometric~~  
504 ~~and fluvial characteristics of the studied region and compare these to existing models of~~  
505 ~~deformation. We also discuss how our new luminescence chronological estimates from the~~  
506 ~~transiently-stored sediment archive help us to constrain fluvial incision rates over Late~~  
507 ~~Pleistocene- Holocene timescale and put them in context to Thus, we have come up with a~~  
508 ~~morphometric analysis of the terrain and combined those results with existing chronology and~~  
509 ~~structural data as a proxy for regional tectonic deformation models- 1. Mid-crustal ramp model~~  
510 ~~vs. 2. Out-of-sequence fault model. the spatial distribution of faulting and fault patterns.~~

511

## 512 **5.1. Knickpoints and their genesis**

513 Already Seeber and Gornitz (1983) ~~had recognized along showed that~~ the Chenab River  
514 is characterized by a zone of steep channel gradient in the vicinity of the KW. [Nennewitz et al.,](#)  
515 ~~(2017)Thiede and Ehlers (2013)~~ demonstrated a strong correlation between steeped longitudinal  
516 river profiles and young thermochronological cooling ages, suggesting recent focused rock uplift  
517 and rapid exhumation along many major rivers draining the southern Himalayan front. Although,  
518 it is still an open debate whether uplift and growth of the LH Duplex are triggered solely by slip  
519 over the crustal ramp of the MHT or additional out-of-sequence surface-breaking faults are  
520 augmenting it (Herman et al., 2010; Elliot et al., 2016; Whipple et al., 2016).

521 The longitudinal profile of the lower Chenab traverse (below ~2000 m above MSL) is  
522 punctuated by two prominent stretches of knickpoint zones ~~and several minor knickpoints related~~  
523 ~~to change of fluvial gradient~~ (Fig.6). Below we will discuss the potential cause of formation of

524 those major knickpoints in the context of detailed field observation, of existing field-collected  
525 structural and lithological data, geomorphic features, rock strength and channel width  
526 information (Fig.7).

### 527 ***5.1.1. Lithologically-controlled knickpoints***

528 Our findings show that the The Himalayan traverse of the Chenab River is characterized  
529 by large variations in substrate lithology and rock strength, which cause variations in the fluvial  
530 erodibility and form knickpoints on the river profile (Fig.1, Fig.7e). ~~These variations have~~  
531 ~~inflicted their ‘marks’ on the river profile.~~ An instance of soft-to-hard substrate transition  
532 happens across the knickpoint L1KP1, lying downstream from the Padder valley, at the eastern  
533 edge of the KW (Fig.2a). Across L1KP1, the river enters the over-deepened LH bedrock gorge  
534 (R value > 50) after exiting the Padder valley filled with transiently-stored, unconsolidated  
535 fluvio-glacial sediments (Fig. 3a). A similar soft-to-hard substrate transition is observed upstream  
536 from the MCT shear zone. The corresponding knickpoint L2KP5 represents a change in  
537 lithological formation from the sheared and deformed Higher Himalayan crystalline (R  
538 value ~35-40) to deep-seated Haimantas (R value ~40-50). There is no field evidence, such as  
539 fault splays or ramps, in support of L2KP5 to be a structurally-controlled one.

### 540 ***5.1.2. Tectonically-controlled knickpoints***

541 Compiling previously-published data on regional tectonogeomorphic attributes (Gavillot  
542 et al., 2018) with detailed field documentation of structural styles and tectonic features; we  
543 identified several stretches where variations in morphometric proxies ~~indicate to constrain~~ spatial  
544 variability in rock uplift and faulting across the KW. We have found at least two instances where  
545 knickzonepoints are not related to change in substrate, nor are they artificially altered such as  
546 constructed dam sites.

547 The knickzone KZ1 (~~upstream marked by KP2~~ ~1700 m above MSL) represents the  
548 upstream reach of a steepened ~~stream segment of run length ~18-20 km. The steep river-~~segment  
549 ~~that~~ represents a drop of ~420m of the Chenab River across a run-length of ~15-20 km (Fig.8c).  
550 The upstream and downstream side of KP21 is characterized by a change in ~~the orientation-~~(dip  
551 ~~angle) of the foliation~~ of the LH bedrock foliation (Fig. 2f, 2g, 8) and channel width (Fig. 7b).  
552 ~~Across K1, the dips of the foliation planes change from ~30° to ~60-65° towards east. K1-KP2~~  
553 also reflects a change in the channel width (Fig. 7b). Interestingly, ~~t~~The steep segment exhibits a  
554 narrower channel and particularly steep valley-walls through the core of the KW. Near the end of  
555 the steep segment, we observed intensely-deformed (folded and fractured) LH rocks are exposed  
556 (Fig.2d, 2e). We infer two ~~There can be two~~ main possibilities for these field observations  
557 combined with systematic changes of geomorphic characteristics such observation— (1) it may  
558 be related to an active surface-breaking out-of-sequence fault or (2) it may be an inactive fault  
559 that defines the floor-thrust of any one of the numerous proposed duplex nappes. ~~We do not find~~  
560 any conclusive evidence of recent activity along this deformed zone, which passively favours the  
561 second possibility. On the contrary, the observed changes in the geomorphic indices along with  
562 stretch of the knickzone KZ1 and observed increase in the bedrock dip angle may well be  
563 explained by a ramp on the basal decollement. This explanation is supported by the existence of  
564 mid-crustal ramps in the balanced cross-section from Gavillot et al., (2018). However, the  
565 structural orientation of the rocks (Fig.8a) differ considerably than the proposed LH duplex in  
566 Gavillot et al., (2008) raising questions about the duplex-model. Our field observations are  
567 supported by works previous studies by~~from~~ Fuchs (1975), Frank et al., (1995) and Stephenson  
568 et al., (2000) who argued against duplexing of multiple thrust nappes and favoured internal  
569 folding of Chail nappe to explain the tectonic for the growth and deformation pattern within of

570 the KW. Therefore, we cannot clearly comment whether K1 represents a transition from flat to  
571 ramp of the MHT or is it indeed an active out-of-sequence thrust-ramp.

572 On the other hand, the other knickpoint KP3 at the upstream-head of KZ22 nearly  
573 coincides with the exposure of the KT (Fig.6). KP32 cannot be a lithologically-controlled  
574 knickpoint as it reflects a hard-to-soft substrate transition from LH rocks (R value > 50) to HH  
575 rocks (R value < 45) (Fig. 7e). We acknowledge that just across the point K2KP3, there are some  
576 strong leucosomatic layers within the migmatites (R: 58±3), but in general, the migmatites are  
577 also brittle-deformed. The rock strength measurement was not done in the multiply-fractured  
578 units as it would show inaccurate values. In the longitudinal profile, K2-KP3 does not represent a  
579 sharp slope break because the downstream segment runs parallel to main structures and KW-  
580 boundary for ~25-30 km ~~and not perpendicular to the orientation of all major structures of the~~  
581 ~~orogen~~, including the KT. Therefore, we performed an orthogonal projection of the E-W trending  
582 traverses of the Chenab River and estimated an orogen-perpendicular drop of the Chenab across  
583 K2-KZ2 (Fig. 8c). The truncated profile across KZ2 shows a drop of ~230m of the channel  
584 across an orogen-perpendicular run-length of ~5 km. The orogen-parallel stretch of the river  
585 exhibits narrow channel width (<30-35m) through moderately hard HH bedrock (R-value: 35-  
586 45). The tributaries within this stretch form significant knickpoint at the confluence with the  
587 trunk stream (Fig.3f). These ~~evidences~~ field observations hint towards ~~asuggest recent~~ rapid  
588 uplift of the ~~HH rocks near the~~ western margin of the KT-KW. The observed differential uplift of  
589 the KW margin and are is possibly either related to growth of the LH-duplex in the core of the  
590 window or by surface expression ~~the presence~~ of another crustal ramp emerging from the MHT  
591 (Fig.8d). ~~Although we didn't find any field evidence of regionally extensive fault along the N-S~~

592 ~~traverse of the Chenab River, similar topographic and morphometric pattern can be caused by an~~  
593 ~~active out-of-sequence fault.~~

594 Both the knickzones, KZ1 and ~~K2-KZ2~~ are the most-prominent disturbance in the  
595 longitudinal profile of the Chenab River and are interpreted to portray spatial distribution of  
596 differential uplift due to tectonic deformation.~~transiently high specific stream power values~~  
597 ~~(Table 1). This signifies the fact that the knickzones are undergoing much rapid fluvial incision~~  
598 ~~than the rest of the study area. If we consider the fluvial incision as a proxy of relative uplift~~  
599 ~~(assuming a steady state), we infer that the knickzones define the spatial extent of the areas~~  
600 ~~undergoing differential uplift caused by movement on the fault ramps.~~

## 601 **5.2.Temporal and spatial variation of fluvial incision across the KW**

602 Bedrock incision in the Himalaya is not a continuous process and is rather controlled by  
603 temporal variations in sediment flux that usually dictates the thickness of the veneer above the  
604 bedrock surfaces over which the rivers flow. Late Pleistocene-Holocene sediment transport  
605 studies suggested an overall climatic control on sediment aggradation in the interiors of the  
606 Himalayan orogen (e.g., Bookhagen et al., 2005; Scherler et al., 2015; Dey et al., 2016); where,  
607 stronger climatic conditions may increase the sediment supply and prompt filling of a river  
608 valley. Transiently-stored valley-fills are re-incised once the climate weakens. Often the re-  
609 incision phases dissect the bedrock units and form strath surfaces. In Chenab valley, we have  
610 documented several stages of valley-fills and fluvial strath surfaces.

611 ~~Epigenetic gorges are common geomorphic features in the high mountain landscape~~  
612 ~~(Quimet et al., 2008). Epigenetic gorges form when channels of a drainage system are buried by~~  
613 ~~sediment aggradation and during subsequent re-incision, a new river channel is incised. The N-S~~  
614 ~~traverse of the Chenab River is largely affected by hillslope sediment flux (paleo-landslides and~~

615 ~~debris flow) from the steep eastern flank. The knickpoint K3 situated near the village of Janwas,~~  
616 ~~mark one such instance of epigenetic gorge where the paleo valley has been filled initially by~~  
617 ~~fluvioglacial sediments and the channel abandonment was caused by landslides and hillslope~~  
618 ~~debris flow prior to 80 kyr (Fig. 4b, 4c).~~

### 619 ***5.2.1. Sediment aggradation in Chenab valley***

620 The Chenab valley records a net sediment aggradation and transient filling of entire  
621 drainage network in the vicinity of the KW since the onset of the last glacial-interglacial cycle  
622 (~130 kyr) till ~80 kyr. Fluvioglacial outwash sediments range from at least ~110-130 kyr,  
623 whereas the hillslope debris ranges from ~90 to ~80 kyr (Table 2). The chronology of the  
624 sediments is in agreement with the overall stratigraphic order of the sediments across the KW.  
625 We observe net fluvial re-incision and formation of bedrock strath surfaces since ~80 kyr and  
626 formation of epigenetic gorges (Fig. 10).

### 627 ***5.3-5.2.2. Drainage re-organization and strath terrace formation along Chenab River***

628 Hillslope debris flow from the high-relief frontal horses of the Lesser Himalayan Duplex  
629 overlies the fluvio-glacial sediments stored beneath the Kishtwar surface. We argue that the  
630 hillslope debris are paleo-landslide deposits which intervened and dammed the paleo-drainage of  
631 the Chenab River, which might have been flowing through an easterly path than now (Fig. 9).  
632 The Maru River, coming from the northwestern corner of our study area was also joining the  
633 Chenab River at a different location (Fig. 9). Our argument is supported by field observation of  
634 thick silt-clay layer in the proposed paleo-valley of the Maru River (Fig. 9a, 9c). OSL sample  
635 (K18) from the silt-clay layer is saturated and hence only provide the minimum age of 52±3 kyr.  
636 We suggest that the hillslope sediment flux dammed the flow of the Chenab River and also  
637 propagated through the aforesaid wind-gap of the Maru River. The decline in the depositional

638 energy has resulted into reduction of grain-size. Post-hillslope debris flow, the Chenab River also  
639 diverted to a new path. The new path of the Chenab River upstream from the confluence with the  
640 Maru River is defined by a very narrow channel flowing through the Higher Himalayan bedrock  
641 gorge (Fig.7b). Downstream from the confluence, we are able to identify at least three levels of  
642 strath terraces lying at heights of ~280-290m (T1), ~170m (T2) and ~120m (T3), respectively  
643 (Fig.3g,10a). Our field observation suggests that the formation of the straths is at least ~52 kyr-  
644 old. The luminescence chronology samples in this study belong to the ~150-170m-thick soft  
645 sediments that are stored stratigraphically-up from the T1 strath level. Our field observations and  
646 chronological estimates suggest that the renewed path of the Chenab River, must have been  
647 formed post the hillslope debris flow ~80-90 kyr but before 52 kyr.

### 648 5.2.3. Knickpoint marking epigenetic gorge

649 Epigenetic gorges are common geomorphic features in the high-mountain landscape  
650 (Ouimet et al., 2008). Epigenetic gorges form when channels of a drainage system are transiently  
651 buried by sediment aggradation and during subsequent re-incision, a new river channel, often  
652 into the neighboring bedrock is incised. The N-S traverse of the Chenab River is largely affected  
653 by hillslope sediment flux (paleo-landslides and debris flow) from the steep eastern flank. The  
654 knickpoint KP4 situated near the village of Janwas, mark one such instance of epigenetic gorge  
655 where the paleo-valley has been filled initially by fluvio-glacial sediments and the channel  
656 abandonment was caused by landslides and hillslope debris flow prior to 80 kyr (Fig.4b, 4c).

### 657

### 658 **5. 43. Rapid bedrock incision along Chenab River on Late Pleistocene timescale**

659 Considering the rate of excavation of softer sediments to be at least an order of magnitude  
660 higher than the rate of bedrock incision (Kothyari and Juyal, 2013; Sharma et al., 2016), we

661 calculated the minimum bedrock incision rate at the western margin of the KW, using the height  
662 of the T1 strath ( $\sim 280 \pm 5$  m) and the average age of the sediments from the Hillslope debris flow  
663 deposit. It yields a minimum bedrock incision rate of  $\sim 3.1$ - $3.5$  mm/yr over the last 80-90 kyr.  
664 Considering the saturated OSL sample from the paleo-valley, we estimated the maximum  
665 bedrock incision since 52 kyr to be 5.1-5.5 mm/yr. Similarly, using the minimum age estimate of  
666 the T3 terrace abandonment, we deduce a maximum bedrock incision rate of  $\sim 5.7$ - $6.1$  mm/yr  
667 since  $\sim 21$  kyr. However, further downstream, away from the KW, the average bedrock incision  
668 rate derived from dated strath surfaces ( $\sim 36 \pm 2$  m high from the Chenab River) near the town of  
669 Doda is  $0.7 \pm 0.1$  mm/yr (sample K01 and K06). We don't have bedrock incision rates from the  
670 core and the eastern margin of the KW, as the core is devoid of sediment storage and the eastern  
671 margin is filled with fluvioglacial sediments and the river is incising the fill. These results  
672 indicate that despite transient choking of the drainage network by sediments during times of  
673 valley aggradation, the topography experienced high incision, when sediment coverage had been  
674 completely penetrated and bedrock straths had been created post-renewal of the fluvial flow.

675

#### 676 **5.54. Findings-Our new results in context with the previously-published data**

677 AFT-cooling ages by Kumar et al., (1995) showcased young cooling ages from the core  
678 of the KW and its western margin (AFT ages:  $\sim 2$ - $3$  Myr) compared to the surroundings (AFT  
679 age: 6-12 Myr). The calculated high exhumation rates proposed by Gavillot et al., (2018) are  
680 based on using a geothermal gradient of  $35$ - $40^\circ\text{C}/\text{km}$  in Dodson's equation assuming a 1-D  
681 model (Dodson, 1973). Additional data and thermal modeling are needed across the KW to  
682 constrain the exhumation rates from vertical transect. However, lateral similarities of the regional  
683 topography and age patterns along the Sutlej area, Beas and Dhauladhar Range (Thiede et al.,

684 | 2017; Thiede et al., 2009; Stübner et al., 2018) have ~~yielded similar~~ yielded similar exhumation  
685 | rates in the range of 2-3 mm/yr and are confirming obtained rates. Long-term exhumation rates  
686 | from the NW Himalaya agree well with findings of Nennewitz et al. (2018) who correlated the  
687 | young thermochron ages with high basinwide  $k_{sn}$  values suggesting high uplift rates over  
688 | intermediate to longer timescales. ~~However, a study from the Sikkim Himalaya by Abrahami et~~  
689 | ~~al., (2016) portrays decoupling between long-term exhumation rates and millennial-scale~~  
690 | ~~basinwide denudation rates. That study highlighted that in high elevation glaciated catchments~~  
691 | ~~the exhumation rates are significantly lower than millennial-scale denudation rates. However, in~~  
692 | ~~case of the NW Himalaya, the proposed range of long-term exhumation rates of ~3 mm/yr mm/y~~  
693 | ~~determined by Gavillot et al., (2018) agree with the regional data pattern.~~ Although the  
694 | geomorphic implications on landscape evolution provide resolution at shorter timescales than the  
695 | low-T thermochron studies, our field observations and analysis support very well a protracted  
696 | long-term uplift rates of across the KW. ~~Unless there has been an ongoing uplift, the geomorphic~~  
697 | ~~signatures would have been subdued. Young low-T AFT ages (Kumar et al., 1995) had been~~  
698 | ~~sampled from the steepened stream reaches, where the SSP is high (Table 1).~~ Interestingly,  
699 | exhumation rates steepened stretches is nearly one order of magnitude higher than that of the  
700 | Higher Himalayan units in the klippe. Our estimates of SSP also reflect an increase by ~five  
701 | times within the steepened stretches.

## 702 | **5.5. Two competing models: duplex-growth model vs. out-of-sequence fault-ramp model**

703 | Deeply-incised channel morphology, steep channel gradients marked by knickpoints at  
704 | the upstream reaches in and around the KW could be explained by the presence of at least two  
705 | orogen-parallel mid-crustal ramps on the MHT (Fig.8d). Existence of two mid-crustal ramps has  
706 | already been shown through sequential balanced cross-sections for the last 10 Myr across the

707 Kashmir Himalaya (Gavillot et al., 2018). The study by Gavillot et al., (2018) focused on duplex  
708 growth model as the balanced cross-section portrays several LH nappes stacked together (Fig.  
709 8d). Translation on the MHT can impart differential uplift of the LH duplex across the two mid-  
710 crustal ramps as ramps would show higher uplift/ exhumation due to higher angle of dip of floor-  
711 thrust of the duplex. Here we provide more detailed information on ~~structural-style~~spatial  
712 distribution of active differential uplift across the KW (Fig.8a, 8d). **Our field observation**  
713 **questions the existence of multiple nappes forming a duplex (Gavillot et al., 2018) and rather**  
714 **favors anticlinal doming of the pervasively-deformed Chail nappe, as suggested by Fuchs (1975)**  
715 **and Stephenson et al., (2000)**. We observe pronounced deformation at the core of the KW (Fig.  
716 2d, 2e) suggesting that this ~~is~~could be related to active faulting, crustal buckling or internal  
717 folding which maintain continuous rock-uplift forcing the Chenab River to incise and ~~prevail~~  
718 maintain the steepened stretch of KZ1. Gavillot et al., (2018) proposed that translation on a mid-  
719 crustal ramp of the MHT and no surface-faulting is driving the uplift at the core of the KW  
720 (Fig.8d). We provide an alternative explanation for the observed steep stream segment at the core  
721 of the KW. One alternative explanation is~~We speculate~~ the existence of a crustal fault-ramp  
722 emerging from the MHT that triggers rapid exhumation of the hanging wall. In ~~this-that~~ case,  
723 out-of-sequence faulting causes high relief, steep channel gradients and higher basinwide  
724 steepness indices over the ramp (Fig.7). Similar ramps have been proposed on the MBT beneath  
725 the Dhauladhar Range (Thiede et al., 2017) and in the east of the NW Himalaya (Caldwell et al.,  
726 2013; Mahesh et al., 2015; Stübner et al., 2018; Yadav et al., 2019). Similar mid-crustal ramp  
727 (MCR-2) has been proposed for the western margin of the KW by Gavillot et al., (2018). We  
728 don't have any direct field evidence of regional surface-breaking faults which could be related to  
729 KZ2-kniekzone. However, ~~a~~rapid fluvial incision, increase in SSP and channel steepness and

730 ~~transient increase in morphometric parameter values~~ probably justify the existence of either a  
731 mid-crustal ramp or an out-of-sequence surface-breaking fault.

732 ~~Our findings from the Kishtwar region of the NW Himalaya establish the importance of~~  
733 ~~morphometric parameters in the assessment of intermediate timescales of  $10^4$ - $10^6$  years. We can~~  
734 ~~resolve regional variations in the tectonic uplift and related landscape evolution by analyzing the~~  
735 ~~topography with high-resolution DEM.~~

736 ~~Models explaining the spatial distribution of the high uplift zone in the interiors of the~~  
737 ~~Himalaya favor the existence of a mid-crustal ramp, which has variable dimension, geometry,~~  
738 ~~and distance from the mountain front along strike of the Himalayan orogeny (Robert et al.,~~  
739 ~~2009). Nennewitz et al., (2018) have proposed that the million year timescale shortening~~  
740 ~~achieved in the interior of the Himalaya near the Sutlej-Beas area in the eastern Himachal~~  
741 ~~Pradesh is caused by accentuated rock uplift over a ramp at a mid-crustal depth of  $\sim$  8-25 km on~~  
742 ~~the MHT. In contrast, studies from the Dhauladhar Range in the north-western Himalaya hints~~  
743 ~~the presence of deep-seated crustal ramp on the MBT and yielded a shortening rate of  $3 \pm 0.5$~~   
744 ~~mm/yr across the MBT over the last 8 Myr and absence of mid-crustal ramp (Deeken et al., 2011;~~  
745 ~~Thiede et al., 2017). The work by Gavillot et al. (2018) favors the existence of at least two mid-~~  
746 ~~crustal ramps beneath the KW (Supplementary Fig.B2). Their suggestion is in agreement with~~  
747 ~~very young AFT cooling ages (1-3 Ma) (Kumar et al., 1995) in the window (Fig.1a). Our data~~  
748 ~~further supports the idea of mid-crustal ramps beneath the Higher Himalayan domain across the~~  
749 ~~Kashmir and NW Himalaya (Webb et al., 2011; Gavillot et al., 2018; Nennewitz et al., 2018) and~~  
750 ~~possibly explains why the seismic hypocenters are clustered in the vicinity of the proposed ramp~~  
751 ~~of MHT. The seismicity is linked to the ongoing deformation of the Lesser Himalayan anticlinal~~  
752 ~~stack or duplex. These studies altogether point out the along-strike variation in the location of the~~

753 ~~rapidly uplifting crustal ramp with respect to the southern Himalayan front. The crustal ramp in~~  
754 ~~the nearby Kangra recess is located beneath the Dhauladhar Range at the main Himalayan front,~~  
755 ~~whereas, in the Himalayan transects situated towards the east and west of Kangra recess, the~~  
756 ~~ramps are located ~100km inside from the MBT. Topographic relief and basinwide mean ksn~~  
757 ~~distribution (Fig.5) hint towards the existence of a lateral ramp in between the Kangra and the~~  
758 ~~Jammu Kashmir Himalayan transects. However, at this moment, we have no conclusive data in~~  
759 ~~support of this claim.~~

760 Detailed structural mapping and morphometric analysis using high-resolution DEM  
761 provide important constraints on the spatial extent of deformation. We are able to resolve the  
762 high-relief Kishtwar Window and the surroundings into two major steep orogen-parallel belts/  
763 zones (Fig. 5e, 8d) - one at the core of the KW could be an active high-angle fault-ramp  
764 emerging from the MHT or a crustal ramp; and the other one observed along the western margin  
765 of the KW could be another ramp on the MHT or a surface-~~breaking~~breaking back-thrust  
766 evolving in relationship to the growth of the LH duplex fault. ~~We suggest that this has two major~~  
767 ~~implications. One, the structural architecture of the MHT is variable along strike of the entire~~  
768 ~~Himalayan orogen. The MHT may have a single or multiple mid-crustal ramps at places and may~~  
769 ~~have none in some transects. Alternatively, there may active out of sequence faulting in the~~  
770 ~~interiors of the Main Himalayan orogen. Secondly~~More importantly, we demonstrate that  
771 Kishtwar Window is still growing and therefore could be the potential source of future seismic  
772 activity.

773 ~~Although we speculate an out-of-sequence fault model for the growth of the KW, there is~~  
774 ~~an important concern regarding this model. Long term crustal shortening estimated from low T~~  
775 ~~thermochron data (Gavillot et al., 2018) and GPS-derived decadal shortening estimates (Stevens~~

776 ~~and Avouac, 2015) imply steady crustal shortening of  $13 \pm 1$  mm/yr. Assessment of late~~  
777 ~~Pleistocene-Holocene crustal shortening across the Sub-Himalayan domain of the Kashmir~~  
778 ~~Himalaya (Gavillot, 2014; Vassallo et al., 2015) suggests that the total Himalayan shortening~~  
779 ~~since late Pleistocene may have been accommodated only within the Sub-Himalaya; therefore,~~  
780 ~~there is no need of additional out-of-sequence faulting in the KW. However, this is again an~~  
781 ~~assumption that the cumulative crustal shortening rate is steady across different timescales.~~

782

## 783 6. Conclusions

784

785 Our field observation and the characteristics of terrain morphology match well with the  
786 spatial pattern of previously-published thermochronological data and indicate that the Kishtwar  
787 Window is undergoing ~~active and focused~~tectonic deformation, uplift and exhumation at present,  
788 on Late Pleistocene-Holocene timescales~~during intermediate timescales~~, and in geological past  
789 since at least the late Miocene. By compiling our new results~~all the results~~ and published records,  
790 we favor the following conclusions:

- 791 1. The Chenab River maintains an over-steepened bedrock channel and a low  
792 channel width irrespective of lithological variations across the KW and beyond,  
793 suggesting ongoing rapid fluvial incision related to active tectonic rock uplift.
- 794 2. Our field observations, morphometric analysis, and rock strength measurements  
795 document that at least two of these major knickzones with steep longitudinal  
796 gradients on the trunk stream are non-lithologic and are likely related to  
797 differential rock uplift. The incision potential (specific stream power) in the  
798 steepened stretches  $\sim 4$ -5 times higher than the surroundings.

799 3. The differential uplift can be explained either by slip on the multiple ramps on the  
800 MHT and exhumation of the duplex floor-thrust or by a combination of slip on the  
801 MHT ramp and active out-of-sequence faulting. As of now, we do not have any  
802 evidence for large-scale out-of-sequence faulting.

803 4. Luminescence chronology of the transiently-stored sediments along the Chenab  
804 River suggests that the valley had been overfilled by sediments of fluvio-glacial  
805 origin as well as by hillslope sediment flux. Massive sediment aggradation during  
806 ~130-80 kyr led to drainage re-organization and bedrock incision leaving behind  
807 strath surfaces.

808 5. The late Quaternary bedrock incision rates near the western margin of the KW are  
809 high 3.1-3.6 mm/yr while away from KW, the incision rates are low (< 1 mm/yr).  
810 ~~We argue that the high fluvial incision rate can potentially be linked to~~  
811 ~~accommodation of crustal shortening either by growth of the duplex or by active~~  
812 ~~out-of-sequence faulting near KT.~~

813 To summarize, our new study reinforces the importance of detailed field observation, and  
814 morphometric analysis in understanding the neotectonic framework of the interiors of the  
815 Himalaya. With additional chronological evidence from the transiently-stored sediments, we  
816 showcase high rates of bedrock incision in the interior of the western Himalaya, which could  
817 potentially be indicative of tectonic control on landscape evolution. However, to solve the debate  
818 of ongoing duplex-growth vs. active out-of-sequence faulting, we would require more field data  
819 on active structures and chronological constraints on deformation rates across potentially-active  
820 structures.

## 821 **Appendix**

822 Additional maps, figures on morphometric analysis and luminescence dating are listed in  
823 Appendix A. Data of rock strength measurements provided in Table C1. Luminescence sample  
824 processing is elaborated in Appendix B.

#### 825 **Code availability**

826 Authors used open-source codes of Topotoolbox and Topographic Analysis Kit Toolbox  
827 for this study.

#### 828 **Data availability**

829 Field data are already provided in Appendix 1. Additional data on luminescence dating  
830 can be provided on request.

#### 831 **Sample availability**

832 Samples used for luminescence dating are already mostly-destroyed, therefore it is  
833 beyond sharing.

#### 834 **Author contribution**

835 S.Dey, the first author, this work and completed the fieldwork, sample processing,  
836 measurements and writing of this manuscript. R. Thiede helped in fieldwork, discussion and  
837 writing of this manuscript. A. Biswas performed the initial morphometric analysis. N.Chauhan  
838 helped in measurement of luminescence signal and assessment of the data. P.Chakravarti  
839 performed the channel width calculations and compiled the rock strength measurements. V. Jain  
840 helped in discussion and writing of the manuscript.

#### 841 **Competing interests**

842 The authors declare that they have no conflict of interest.

843

#### 844 **Acknowledgments**

845 This study is funded by the DST INSPIRE faculty fellowship program by the Department  
846 of Science and Technology, India (grant #DST/INSPIRE/04/2017/003278), and IIT Gandhinagar  
847 post-doctoral research fund (IP/IITGN/ES/SD/201718-01). Thiede is supported by German  
848 Science Foundation (grant # DFG TH 1317-8 and 9). We thank M.K.Jaiswal and M.Rawat for  
849 providing the elemental analysis. We thank Shambhu Das, Avi Das, Niklas Schaaf, Akashsingh  
850 Rajput and Chamel Singh for their assistance during fieldwork. We also thank Soumyajit  
851 Mukherjee, Rahul Kaushal and Shantamoy Guha for scientific inputs and comments on this  
852 manuscript. We acknowledge A. Forte, Y. Gavillot, ~~and~~ S. Hergarten and one anonymous  
853 reviewer for their constructive and insightful reviews. We like to thank the editor R. Gloaguen  
854 and associate editor A. Joshua West for their help during review process.

855

## 856 **References**

857 Abrahami, R., van der Beek, P., Huyghe, P., Hardwick, E., & Carcaillet, J. (2016). Decoupling of  
858 long-term exhumation and short-term erosion rates in the Sikkim Himalaya. Earth and Planetary  
859 Science Letters, 433, 76-88.

860 ~~Ahnert, F. (1970). Functional relationships between denudation, relief, and uplift in large, mid-~~  
861 ~~latitude drainage basins. American Journal of Science, 268(3), 243-263.~~

862 Bagnold, R. A. (1966). An approach to the sediment transport problem from general physics. US  
863 government printing office.

864 Bhatia, T. R., & Bhatia, S. K. (1973). Sedimentology of the slate belt of Ramban-Banihal area,  
865 Kashmir Himalaya. Himalayan Geology, 3, 116-134.

866 Bollinger, L., Henry, P., & Avouac, J. P. (2006). Mountain building in the Nepal Himalaya:  
867 Thermal and kinematic model. *Earth and Planetary Science Letters*, 244(1-2), 58-71.

868 Bookhagen, B., & Burbank, D. W. (2006). Topography, relief, and TRMM-derived rainfall  
869 variations along the Himalaya. *Geophysical Research Letters*, 33(8).

870 Bookhagen, B., Thiede, R. C., & Strecker, M. R. (2005). Late Quaternary intensified monsoon  
871 phases control landscape evolution in the northwest Himalaya. *Geology*, 33(2), 149-152.

872 Bookhagen, B., Fleitmann, D., Nishiizumi, K., Strecker, M. R., & Thiede, R. C. (2006).  
873 Holocene monsoonal dynamics and fluvial terrace formation in the northwest Himalaya,  
874 India. *Geology*, 34(7), 601-604.

875 Burbank, D. W., Leland, J., Fielding, E., Anderson, R. S., Brozovic, N., Reid, M. R., & Duncan,  
876 C. (1996). Bedrock incision, rock uplift and threshold hillslopes in the northwestern  
877 Himalayas. *Nature*, 379(6565), 505.

878 Burgess, W. P., Yin, A., Dubey, C. S., Shen, Z. K., & Kelty, T. K. (2012). Holocene shortening  
879 across the Main Frontal Thrust zone in the eastern Himalaya. *Earth and Planetary Science*  
880 *Letters*, 357, 152-167.

881 Caldwell, W. B., Klemperer, S. L., Lawrence, J. F., and Rai, S. S., 2013, Characterizing the Main  
882 Himalayan Thrust in the Garhwal Himalaya, India with receiver function CCP stacking: *Earth*  
883 *and Planetary Science Letters*, v. 367, p. 15-27.

884 Colleps, C. L., Stockli, D. F., McKenzie, N. R., Webb, A. A. G., & Horton, B. K. (2019).  
885 Neogene Kinematic Evolution and Exhumation of the NW India Himalaya: Zircon Geo-and

886 Thermochronometric Insights From the Fold-Thrust Belt and Foreland Basin. *Tectonics*, 38(6),  
887 2059-2086.

888 DeCelles, P. G., Robinson, D. M., Quade, J., Ojha, T. P., Garzzone, C. N., Copeland, P., and  
889 Upreti, B. N., 2001, Stratigraphy, structure, and tectonic evolution of the Himalayan fold-thrust  
890 belt in western Nepal: *Tectonics*, v. 20, no. 4, p. 487-509.

891 Deeken, A., Thiede, R. C., Sobel, E. R., Hourigan, J. K., & Strecker, M. R. (2011).  
892 Exhumational variability within the Himalaya of northwest India. *Earth Planetary Science Letters*,  
893 305(1-2), 103–114. <https://doi.org/10.1016/j.epsl.2011.02.045>

894 Dey, S., Thiede, R. C., Schildgen, T. F., Wittmann, H., Bookhagen, B., Scherler, D., & Strecker,  
895 M. R. (2016). Holocene internal shortening within the northwest Sub-Himalaya: Out-of-  
896 sequence faulting of the Jwalamukhi Thrust, India. *Tectonics*, 35(11), 2677-2697.

897 [Dey, S., Thiede, R. C., Schildgen, T. F., Wittmann, H., Bookhagen, B., Scherler, D., Jain, V., &](#)  
898 [Strecker, M. R. \(2016\). Climate-driven sediment aggradation and incision since the late](#)  
899 [Pleistocene in the NW Himalaya, India. \*Earth and Planetary Science Letters\*, 449, 321-331.](#)

900 DiPietro, J. A., & Pogue, K. R. (2004). Tectonostratigraphic subdivisions of the Himalaya: A  
901 view from the west. *Tectonics*, 23(5).

902 Duvall, A., Kirby, E., & Burbank, D. (2004). Tectonic and lithologic controls on bedrock  
903 channel profiles and processes in coastal California. *Journal of Geophysical Research: Earth*  
904 *Surface*, 109(F3).

905 Elliott, J. R., Jolivet, R., González, P. J., Avouac, J. P., Hollingsworth, J., Searle, M. P., &  
906 Stevens, V. L. (2016). Himalayan megathrust geometry and relation to topography revealed by  
907 the Gorkha earthquake. *Nature Geoscience*, 9(2), 174.

908 Eugster, P., Scherler, D., Thiede, R. C., Codilean, A. T., and Strecker, M. R., (2016). Rapid Last  
909 Glacial Maximum deglaciation in the Indian Himalaya coeval with midlatitude glaciers: New  
910 insights from <sup>10</sup>Be-dating of ice-polished bedrock surfaces in the Chandra Valley, NW  
911 Himalaya: *Geophysical Research Letters*, v. 43, no. 4, p. 1589-1597.

912 Finnegan, N. J., Roe, G., Montgomery, D. R., & Hallet, B. (2005). Controls on the channel width  
913 of rivers: Implications for modeling fluvial incision of bedrock. *Geology*, 33(3), 229-232.

914 Flint, J. J. (1974). Stream gradient as a function of order, magnitude, and discharge. *Water*  
915 *Resources Research*, 10(5), 969-973.

916 Forte, A.M. and Whipple, K.X. (2019). The Topographic Analysis Toolkit (TAK) for  
917 Topotoolbox. *Earth Surface Dynamics*, 7, 87-95.

918 Frank, W., Grasemann, B., Guntli, P. E. T. E. R., & Miller, C. (1995). Geological map of the  
919 Kishtwar-Chamba-Kulu region (NW Himalayas, India). *Jahrbuch der Geologischen*  
920 *Bundesanstalt*, 138(2), 299-308.

921 Fuchs, G. (1975). Contributions to the geology of the North-Western Himalayas. *Geologische*  
922 *Bundesanstalt*.

923 Fuchs, G. (1981). Outline of the geology of the Himalaya. *Mitt. osterr. geol. Ges*, 74(75), 101-  
924 127.

925 Gavillot, Y. G. (2014). Active tectonics of the Kashmir Himalaya (NW India) and earthquake  
926 potential on folds, out-of-sequence thrusts, and duplexes.

927 Gavillot, Y., Meigs, A. J., Sousa, F. J., Stockli, D., Yule, D., & Malik, M. (2018). Late Cenozoic  
928 Foreland-to-Hinterland Low-Temperature Exhumation History of the Kashmir  
929 Himalaya. *Tectonics*.

930 Gavillot, Y., Meigs, A., Yule, Y., Heermance, R., Rittenour, T., Madugo, C., & Malik, M.  
931 (2016). Shortening rate and Holocene surface rupture on the Riasi fault system in the Kashmir  
932 Himalaya: Active thrusting within the Northwest Himalayan orogenic wedge. *Geological Society  
933 of America Bulletin*, 128(7-8), 1070–1094. <https://doi.org/10.1130/B31281.1>

934 Harvey, J. E., Burbank, D. W., & Bookhagen, B. (2015). Along-strike changes in Himalayan  
935 thrust geometry: Topographic and tectonic discontinuities in western Nepal. *Lithosphere*, 7(5),  
936 511-518.

937 Herman, F., Copeland, P., Avouac, J.P., Bollinger, L., Mahéo, G., Le Fort, P., Rai, S., Foster, D.,  
938 Pêcher, A., Stüwe, K. and Henry, P., 2010. Exhumation, crustal deformation, and thermal  
939 structure of the Nepal Himalaya derived from the inversion of thermochronological and  
940 thermobarometric data and modeling of the topography. *Journal of Geophysical Research: Solid  
941 Earth*, 115(B6).

942 Hirschmiller, J., Grujic, D., Bookhagen, B., Coutand, I., Huyghe, P., Mugnier, J.-L., and Ojha,  
943 T., 2014, What controls the growth of the Himalayan foreland fold-and-thrust belt?: *Geology*, v.  
944 42, no. 3, p. 247-250.

945 Kaushal, R. K., Singh, V., Mukul, M., & Jain, V. (2017). Identification of deformation  
946 variability and active structures using geomorphic markers in the Nahan salient, NW Himalaya,  
947 India. *Quaternary International*, 462, 194-210.

948 Kumar, A., Lal, N., Jain, A. K., & Sorkhabi, R. B. (1995). Late Cenozoic–Quaternary thermo-  
949 tectonic history of Higher Himalayan Crystalline (HHC) in Kishtwar–Padar–Zaskar region,  
950 NW Himalaya: Evidence from fission-track ages. *Journal of the Geological Society of India*,  
951 45(4), 375–391.

952 Kundu, B., Yadav, R. K., Bali, B. S., Chowdhury, S., & Gahalaut, V. K. (2014). Oblique  
953 convergence and slip partitioning in the NW Himalaya: implications from GPS  
954 measurements. *Tectonics*, 33(10), 2013-2024.

955 Lavé, J., & Avouac, J. P. (2000). Active folding of fluvial terraces across the Siwaliks Hills,  
956 Himalayas of central Nepal. *Journal of Geophysical Research: Solid Earth*, 105(B3), 5735-5770.

957 Lavé, J., & Avouac, J. P. (2001). Fluvial incision and tectonic uplift across the Himalayas of  
958 central Nepal. *Journal of Geophysical Research: Solid Earth*, 106(B11), 26561-26591.

959 Mahesh, P., Gupta, S., Saikia, U., and Rai, S. S., 2015, Seismotectonics and crustal stress field in  
960 the Kumaon-Garhwal Himalaya: *Tectonophysics*, v. 655, p. 124-138.

961 Malik, J. N., & Mohanty, C. (2007). Active tectonic influence on the evolution of drainage and  
962 landscape: geomorphic signatures from frontal and hinterland areas along the Northwestern  
963 Himalaya, India. *Journal of Asian Earth Sciences*, 29(5-6), 604-618.

964 Miller, J. R. (1991). The influence of bedrock geology on knickpoint development and channel-  
965 bed degradation along downcutting streams in south-central Indiana. *The Journal of*  
966 *Geology*, 99(4), 591-605.

967 Mitra, G., Bhattacharyya, K., & Mukul, M. (2010). The lesser Himalayan duplex in Sikkim:  
968 implications for variations in Himalayan shortening. *Journal of the Geological Society of*  
969 *India*, 75(1), 289-301.

970 Montgomery, D. R., & Brandon, M. T. (2002). Topographic controls on erosion rates in  
971 tectonically active mountain ranges. *Earth and Planetary Science Letters*, 201(3-4), 481-489.

972 Mukherjee S. (2015) A review on out-of-sequence deformation in the Himalaya. In: Mukherjee  
973 S, Carosi R, van der Beek P, Mukherjee BK, Robinson D (Eds) *Tectonics of the*  
974 *Himalaya*. Geological Society, London. Special Publications 412, 67-109.

975 Nábělek, J., Hetényi, G., Vergne, J., Sapkota, S., Kafle, B., Jiang, M., Su, H., Chen, J., & Huang,  
976 B. S. (2009). Underplating in the Himalaya-Tibet collision zone revealed by the Hi-CLIMB  
977 experiment. *Science*, 325(5946), 1371-1374.

978 Nadim, F., Kjekstad, O., Peduzzi, P., Herold, C., & Jaedicke, C. (2006). Global landslide and  
979 avalanche hotspots. *Landslides*, 3(2), 159-173.

980 Nennowitz, M., Thiede, R. C., & Bookhagen, B. (2018). Fault activity, tectonic segmentation,  
981 and deformation pattern of the western Himalaya on Ma timescales inferred from landscape  
982 morphology. *Lithosphere*, 10(5), 632-640.

983 Ni, J., and M. Barazangi (1984), Seismotectonics of the Himalayan collision zone: Geometry of  
984 the underthrusting Indian plate beneath the Himalaya, *J. Geophys. Res.*, 89, 1147 – 1163.

985 ~~Paul, H., Priestley, K., Powali, D., Sharma, S., Mitra, S., & Wanchoo, S. (2018). Signatures of the~~  
986 ~~existence of frontal and lateral ramp structures near the Kishtwar Window of the Jammu and~~  
987 ~~Kashmir Himalaya: Evidence from microseismicity and source mechanisms. *Geochemistry,*~~  
988 ~~*Geophysics, Geosystems*, 19(9), 3097-3114.~~

989 ~~Phartiyal, B., Sharma, A., Srivastava, P., & Ray, Y. (2009). Chronology of relict lake deposits in~~  
990 ~~the Spiti River, NW Trans Himalaya: Implications to Late Pleistocene-Holocene climate~~  
991 ~~tectonic perturbations. *Geomorphology*, 108(3-4), 264-272.~~

992 Powers, P. M., Lillie, R. J., & Yeats, R. S. (1998). Structure and shortening of the Kangra and  
993 Dehra Dun reentrants, sub-Himalaya, India. *Geological Society of America Bulletin*, 110(8),  
994 1010-1027.

995 Raiverman, V. (1983). Basin geometry, Cenozoic sedimentation and hydrocarbon prospects in  
996 north western Himalaya and Indo-Gangetic plains. *Petroleum Asia Journal: Petroliferous basins*  
997 *of India*, 6(4), 67-92.

998 Robert, X., Van Der Beek, P., Braun, J., Perry, C., Dubille, M., & Mugnier, J. L. (2009).  
999 Assessing Quaternary reactivation of the Main Central thrust zone (central Nepal Himalaya):  
1000 New thermochronologic data and numerical modeling. *Geology*, 37(8), 731-734.

1001 Robinson, D. M., & Martin, A. J. (2014). Reconstructing the Greater Indian margin: A balanced  
1002 cross section in central Nepal focusing on the Lesser Himalayan duplex. *Tectonics*, 33(11), 2143-  
1003 2168.

1004 Royden, L., & Taylor Perron, J. (2013). Solutions of the stream power equation and application  
1005 to the evolution of river longitudinal profiles. *Journal of Geophysical Research: Earth*  
1006 *Surface*, 118(2), 497-518.

1007 Scherler, D., Bookhagen, B., Wulf, H., Preusser, F., & Strecker, M. R. (2015). Increased late  
1008 Pleistocene erosion rates during fluvial aggradation in the Garhwal Himalaya, northern  
1009 India. *Earth and Planetary Science Letters*, 428, 255-266.

1010 Schwanghart, W., & Scherler, D. (2014). TopoToolbox 2—MATLAB-based software for  
1011 topographic analysis and modeling in Earth surface sciences. *Earth Surface Dynamics*, 2(1), 1-7.

1012 Searle, M. P., Stephenson, B., Walker, J., & Walker, C. (2007). Restoration of the Western  
1013 Himalaya: implications for metamorphic protoliths, thrust and normal faulting, and channel flow  
1014 models. *Episodes*, 30(4), 242.

1015 Seeber, L., & Gornitz, V. (1983). River profiles along the Himalayan arc as indicators of active  
1016 tectonics. *Tectonophysics*, 92(4), 335-367.

1017 Snyder, N. P., Whipple, K. X., Tucker, G. E., & Merritts, D. J. (2000). Landscape response to  
1018 tectonic forcing: Digital elevation model analysis of stream profiles in the Mendocino triple  
1019 junction region, northern California. *Geological Society of America Bulletin*, 112(8), 1250-1263.

1020 Steck, A. (2003). Geology of the NW Indian Himalaya. *Eclogae Geol Helv*, 96, 147-196.

1021 Stephenson, B. J., Waters, D. J., & Searle, M. P. (2000). Inverted metamorphism and the Main  
1022 Central Thrust: field relations and thermobarometric constraints from the Kishtwar Window, NW  
1023 Indian Himalaya. *Journal of Metamorphic Geology*, 18(5), 571-590.

1024 Stevens, V. L., & Avouac, J. P. (2015). Interseismic coupling on the main Himalayan  
1025 thrust. *Geophysical Research Letters*, 42(14), 5828-5837.

1026 Stübner, K., Grujic, D., Dunkl, I., Thiede, R., & Eugster, P. (2018). Pliocene episodic  
1027 exhumation and the significance of the Munsiri thrust in the northwestern Himalaya. *Earth and*  
1028 *Planetary Science Letters*, 481, 273-283.

1029 Thakur, V. C. (Ed.). (1992). *Geology of western Himalaya* (Vol. 19). Pergamon Press.

1030 Thakur, V. C., Joshi, M., Sahoo, D., Suresh, N., Jayangondapermal, R., & Singh, A. (2014).  
1031 Partitioning of convergence in Northwest Sub-Himalaya: estimation of late Quaternary uplift and  
1032 convergence rates across the Kangra reentrant, North India. *International Journal of Earth*  
1033 *Sciences*, 103(4), 1037-1056.

1034 Thiede, R., Robert, X., Stübner, K., Dey, S., & Faruhn, J. (2017). Sustained out-of-sequence  
1035 shortening along a tectonically active segment of the Main Boundary thrust: The Dhauladhar  
1036 Range in the northwestern Himalaya. *Lithosphere*, 9(5), 715-725.

1037 Thiede, R. C., Bookhagen, B., Arrowsmith, J. R., Sobel, E. R., & Strecker, M. R. (2004).  
1038 Climatic control on rapid exhumation along the southern Himalayan Front. *Earth and Planetary*  
1039 *Science Letters*, 222(3-4), 791–806. <https://doi.org/10.1016/j.epsl.2004.03.015>

1040 Turowski, J. M., Lague, D., and Hovius, N. (2009). Response of bedrock channel width to  
1041 tectonic forcing: Insights from a numerical model, theoretical considerations, and comparison  
1042 with field data. *Journal of Geophysical Research: Earth Surface*, 114(F3).

1043 Vassallo, R., Mugnier, J. L., Vignon, V., Malik, M. A., Jayangondaperumal, R., Srivastava, P.,  
1044 and Carcaillet, J. (2015). Distribution of the late-Quaternary deformation in northwestern  
1045 Himalaya. *Earth and Planetary Science Letters*, 411, 241-252.

1046 Wadia, D. N. (1934). The Cambrian-Trias sequence of north-western Kashmir (parts of  
1047 Muzaffarabad and Baramula districts). *Records of the Geological Survey of India*, 68(2), 121-  
1048 176.

1049 Webb, A. A. G., Yin, A., Harrison, T. M., C  l  rier, J., Gehrels, G. E., Manning, C. E., & Grove,  
1050 M. (2011). Cenozoic tectonic history of the Himachal Himalaya (northwestern India) and its  
1051 constraints on the formation mechanism of the Himalayan orogen. *Geosphere*, 7(4), 1013-1061.

1052 Wesnousky, S. G., Kumar, S., Mohindra, R., & Thakur, V. C. (1999). Uplift and convergence  
1053 along the Himalayan Frontal Thrust of India. *Tectonics*, 18(6), 967-976.

1054 Whipple, K. X., & Tucker, G. E. (1999). Dynamics of the stream-power river incision model:  
1055 Implications for height limits of mountain ranges, landscape response timescales, and research  
1056 needs. *Journal of Geophysical Research: Solid Earth*, 104(B8), 17661-17674.

1057 Whipple, K. X., DiBiase, R. A., & Crosby, B. T. (2013). Bedrock rivers. In *Treatise on*  
1058 *geomorphology*. Elsevier Inc..

1059 Wobus, C. W., Hodges, K. V., & Whipple, K. X. (2003). Has focused denudation sustained  
1060 active thrusting at the Himalayan topographic front?. *Geology*, 31(10), 861-864.

1061 Wobus, C., Heimsath, A., Whipple, K., & Hodges, K. (2005). Active out-of-sequence thrust  
1062 faulting in the central Nepalese Himalaya. *Nature*, 434(7036), 1008.

1063 Wobus, C., Whipple, K. X., Kirby, E., Snyder, N., Johnson, J., Spyropolou, K., Crosby, B.,  
1064 Sheehan, D & Willett, S. D. (2006). Tectonics from topography: Procedures, promise, and  
1065 pitfalls. *Special papers-geological society of America*, 398, 55.

1066 Yadav, R. K., Gahalaut, V. K., Bansal, A. K., Sati, S., Catherine, J., Gautam, P., Kumar, K., and  
1067 Rana, N., 2019, Strong seismic coupling underneath Garhwal–Kumaun region, NW Himalaya,  
1068 India: Earth and Planetary Science Letters, v. 506, p. 8-14.

1069 Yin, A., & Harrison, T. M. (2000). Geologic evolution of the Himalayan-Tibetan orogen. Annual  
1070 Review of Earth and Planetary Sciences, 28(1), 211-280.

1071

1072 **Figure captions**

1073

1074 **Figure 1:** (a) An overview geological map of the western sector of the Indian Himalaya showing  
1075 major lithology (modified after Steck, 2003 and Gavillot et al., 2018) and existing structures  
1076 (Vassalo et al., 2015; Gavillot et al., 2018). The tectonic Kishtwar Window (KW) is surrounded  
1077 by exposure of MCT, locally known as the Kishtwar Thrust (KT), and exposes the Lesser  
1078 Himalayan nappes. The Lesser Himalaya forms a west-verging asymmetric anticline. Apatite  
1079 fission-track (AFT) ages are adapted from Kumar et al., (1995). (b) A balanced cross-section of  
1080 the NW Himalaya showing the general architecture of the Himalayan orogenic wedge (modified  
1081 after Gavillot et al., 2018). Note that, beneath the KW, Gavillot et al., (2018) proposed the  
1082 existence of at least two crustal ramps (MCR-1 and MCR-2) on the MHT, translation on which  
1083 may have resulted in 3.2-3.6 mm/yr Quaternary exhumation rates across the KW.

1084 **Figure 2:** Lithological units and structural orientations observed in the Chenab valley. (a)  
1085 Steeply-dipping HHCS units near the western margin of the KW. (b) Highly-deformed  
1086 migmatites at the base of the KT. (c) Sub-vertical quartzite slabs of Chail Formation exposed in  
1087 the frontal horses of the LH Duplex (or, anticline). (d) Highly-deformed, sub-vertical and  
1088 pervasively folded and compressed quartzite layers within the core of the KW, the base of

1089 stacked LH-nappes forming the hanging wall of the proposed surface-breaking fault (Fig. 8d). (e)  
1090 A close-up view of the folded quartzite units. (f) Steeply-dipping units of granite which formed  
1091 new penetrative foliation outcropping upstream from the fault-zone. (g) Further upstream from  
1092 the fault-zone, the bedrocks are gentler in the eastern edge of the KW.

1093 **Figure 3:** Figure 3: Geomorphic features observed along the Chenab River across the KW. (a)  
1094 Where the Chenab River enters the KW, the major tributaries coming from the Zansar Range in  
1095 the north are characterized by ‘U-shaped’ valley suggesting repeated glacial occupancy during  
1096 the Quaternary. The Chenab valley is unusually wide here providing space for transient storage  
1097 of glacial outwash sediments. The present-day River re-incises these sedimentary fills.  
1098 Photograph was taken near the town of Padder (cf. Fig.1a). (b) At the core of the KW, the  
1099 Chenab valley is V-shaped, steep The Chenab River is steep and maintains a narrow channel  
1100 width. (c) Highly-elevated fluvial strath surfaces are preserved in the vicinity of the town of  
1101 Kishtwar Fluvial incision observed along the N-S traverse of the Chenab River. Photograph was  
1102 taken from south of the Kishtwar town. The Kishtwar surface (~400m high from the river) is  
1103 underlain by ~150-170m thick sediment cover overlying the tilted Higher Himalayan bedrock.  
1104 The River has incised another ~240m bedrock in this section. (d) Epigenetic gorge formed along  
1105 the Chenab River in its’ N-S traverse through the HHCS. The town of Drabshalla is built on the  
1106 hillslope deposits. (e) Chenab River maintained very narrow channel (width: ~20-25 m) through  
1107 moderately-strong HHCS rocks, suggesting tectonic imprint on topography. (f) Formation of  
1108 knickpoint at the confluence of the tributary with the trunk stream implying rapid fluvial incision  
1109 of the trunk stream. (g) Three levels of strath surfaces observed below the Kishtwar surface. The  
1110 strath levels are marked as T1 (~280m), T2 (~170m) and T3 (~120m). OSL dating of fluvial  
1111 sediments lying above the T3 surface yield a minimum depositional age of  $\sim 21.6 \pm 2.6$  ky.

1112 **Figure 4:** (a) Lithological distribution near the western margin of the KW (cf. Fig.8 for  
1113 location). Luminescence sample (OSL and IRSL) locations and respective depositional ages (in  
1114 kyr) are shown. Every sample except K16 and K17 are taken above strath level T1. K16 and  
1115 K17 are taken from above the T3 level. Note that, the ages reported in italics are minimum age  
1116 estimates. (b) A field photograph from the village Janwas, south of the town of Kishtwar,  
1117 showing the aggraded sediments lying above the Higher Himalayan tilted bedrock units. (c)  
1118 IRSL ages (in kyr) from the fluvio-glacial sediments and OSL age (in kyr) from the hillslope  
1119 debris units suggest the valley aggradation probably started at the transition of the glacial to  
1120 interglacial phase ~120-130 kyr and continued till ~80 kyr ago. (d) A close-up view (red  
1121 rectangle in fig.4c) of the tilted fluvio-glacial sediment layers showing alternate conglomerate and  
1122 medium-coarse sand layers. (e) A ~3m thick fine sand layer within the hillslope debris yield  
1123 depositional age of  $\sim 86 \pm 5$  kyr. Photograph was taken near the village Pochal, northwest of the  
1124 town of Kishtwar.

1125 **Figure 5:** Regional variations in (a) topography, (b) topographic relief (moving window of ~4  
1126 km) (c) TRMM-derived rainfall (after Bookhagen and Burbank, 2006), and (d) Basinwide  
1127 Normalized steepness indices (ksn value) of the region shown dashed box in Figure 1a. (e)  
1128 Swath profiles (swath window: 50 km) along the line AB (cf. Fig.5a) demonstrate the orogen-  
1129 perpendicular variations in elevation, rainfall and ksn value. KW is characterized by high  
1130 elevation, high relief and high steepness, but low rainfall.

1131 **Figure 6:** Longitudinal profile of the Chenab River show major changes in channel gradient  
1132 associated with knickpoints in the upstream. It illustrates the major changes in the channel  
1133 gradient extend over the full length of the KW and strongest changes are located in the core and  
1134 not at the margins of the window. We classified knickpoints on the basis of their genesis. The

1135 substrate lithology along the River is shown. Knickpoints caused by glacial occupancy (G1, G2  
1136 and G3) are adapted from Eugster et al., (2016), who reconstructed the timing of maximum  
1137 glaciation and extent of glacial cover in source region of upper Chenab River basin during the  
1138 last glacial maximum. These knickpoints highlight the importance of glacial erosion in the high-  
1139 elevation sectors, especially in the northern tributaries of the Chenab River. Further in this study,  
1140 we focused on the area marked by red rectangle.

1141 **Figure 7:** Along-river variations in (a) channel-elevation, (b) channel width, (c) channel  
1142 gradient, (d) Normalized steepness index, and (e) rock-strength of non-fractured bedrock units  
1143 (R-value taken by rebound hammer) till 165 km upstream from the MBT (point X, cf. Fig.1a).  
1144 The mean  $R\text{-value} \pm \sigma$  for each rock type has been plotted against their spatial extent. We  
1145 identified two distinct zones (K1 and K2) of high channel gradient and steepness index, which  
1146 maintain low channel width despite the variable rock strength of the substrate. Knickpoint **K3**  
1147 **KP4** may have been generated by the formation of the epigenetic gorge along the N-S traverse of  
1148 the Chenab River (cf. Fig.3c). Knickpoints **L1KP1** and **L2KP5** mark the transition of a soft-to-  
1149 hard bedrock substrate.

1150 **Figure 8:** (a) Detailed structural data from the study area showing structural and lithological  
1151 variations (modified after Steck, 2003; Gavillot et al., 2018). (b) and (c) orogen-perpendicular  
1152 drop of the Chenab trunk stream across stretch 1 and stretch 2, respectively, showing transient  
1153 increase in steepness over the K1 and K2 knickzone. The orthogonal profile projection method  
1154 has been used in the case of K2 (cf. fig.7) to identify the width of the steep segment. (d)  
1155 Comparison between two deformation models explaining the observed morphometric variations  
1156 across the KW – (a) duplex-growth model (adapted from Gavillot et al., 2018) and (b) active out-  
1157 of-sequence fault model.

1158 **Figure 9:** A satellite image of the northern Kishtwar town showing the present-day flow-path of  
1159 the Chenab River (cf. Fig.8 for location). Hillslope debris originated from the steep western  
1160 margin of the KW (only made of massive white quartzites) and was deposited over fluvio-glacial  
1161 and glacio-lacustrine sediments and Higher Himalaya schists bedrock exposed below in the  
1162 Kishtwar valley. Massive hillslope sediment flux impeded the paleo-drainage system leaving  
1163 behind the paleo-valley of the tributary, the Maru River. Our interpretation of the paleo-drainage  
1164 is marked in a white dashed line. (a) A view of the Kishtwar surface from the western margin  
1165 of the KW showing present-day gorge of the Chenab River and its tributary. The wind-gap  
1166 (paleo-valley) of the tributary is visible. (b) Thick clay-silt deposit in the wind-gap suggests  
1167 abandonment of river-flow. The OSL sample is saturated and hence only denotes the minimum  
1168 age of valley abandonment/ hillslope debris flow. (c) Overview picture of the frontal horses of  
1169 the LH duplex and the direction of debris flow towards the Kishtwar town. (d) Angular, poorly-  
1170 sorted clasts and boulders were observed at the base of the debris flow unit near the village of  
1171 Pochal, north of the Kishtwar town. The white quartzites of LH are exposed in the vicinity of the  
1172 Kishtwar Town (see satellite image) – only the eastern valley flank can have collapsed in the  
1173 past.

1174 **Figure 10:** (a) A topographic and geomorphic profile across the Chenab valley drawn over the  
1175 Kishtwar Town. The valley aggradation by fluvio-glacial and hillslope debris sediments was  
1176 succeeded by a fluvial incision which penetrated through the unconsolidated sediments of  
1177 thickness ~140-150m and incised Higher Himalayan bedrock by  $\sim 280 \pm 5$  m, leaving behind at  
1178 least three recognizable strath surfaces with a thin late Pleistocene sediment cover. The three  
1179 strath surfaces are at  $280 \pm 5$  m (T1),  $\sim 170$  m (T2), and  $\sim 120 \pm 5$  m (T3) heights from the present-  
1180 day River. We assume that the present-day bedrock gorge has been carved since the deposition

1181 of the glacio-lacustrine sediment deposits (~100-130 ky) and the hillslope debris (~90-80 ky)  
1182 onto former fluvial strath surface of Higher Himalayan Bedrock. The width of the fluvial strath  
1183 surface where the Kishtwar Town is located indicates that the river network had been dammed  
1184 earlier too. (b) Graphical representation of mean bedrock incision rates since 80 kyr. Age  
1185 constraints for T3 are shown in Fig. 4a. Based on relative heights and depositional ages of late  
1186 Pleistocene deposits, we propose a minimum and a maximum bedrock incision rate of 3.1-3.5  
1187 mm/y and 5.2-5.6 mm/yr, respectively. However, further downstream, the bedrock incision rates  
1188 calculated from bedrock straths farther downstream from the KW range 0.7-0.8 mm/yr.

1189 **Table caption:**

1190 **Table 1:** Calculations of change in specific stream power (SSP) values across the ramp and the  
1191 flat segments beneath the LH Duplex. We used a uniform discharge for SSP calculation.

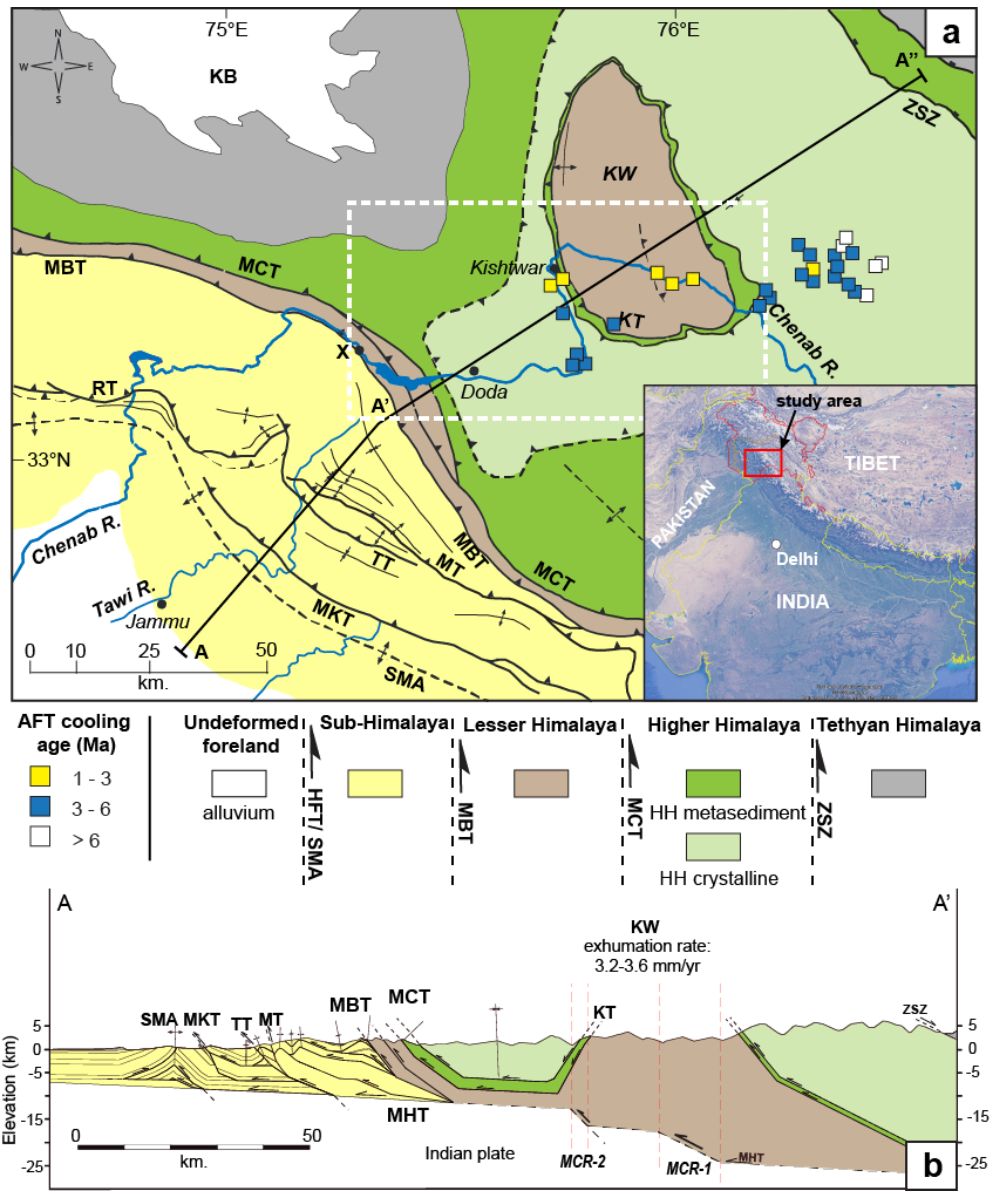
1192 **Table 2:** Sample locations, elemental concentrations, dose rates, equivalent doses and age  
1193 estimations for sand samples from Kishtwar valley.

1194

1195 Figures

1196

Figure 1



1197

1198

1199

Figure 2

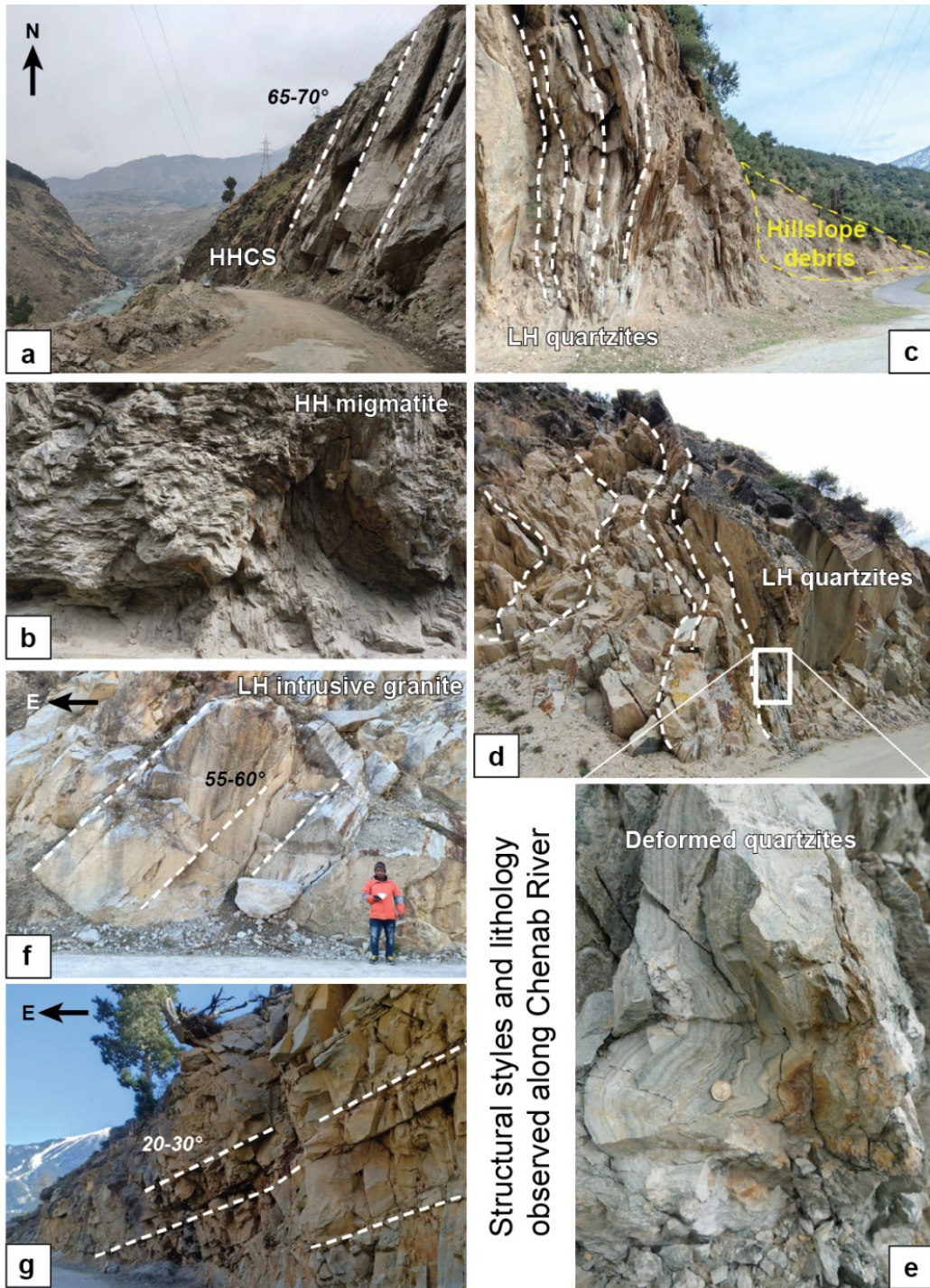


Figure 3

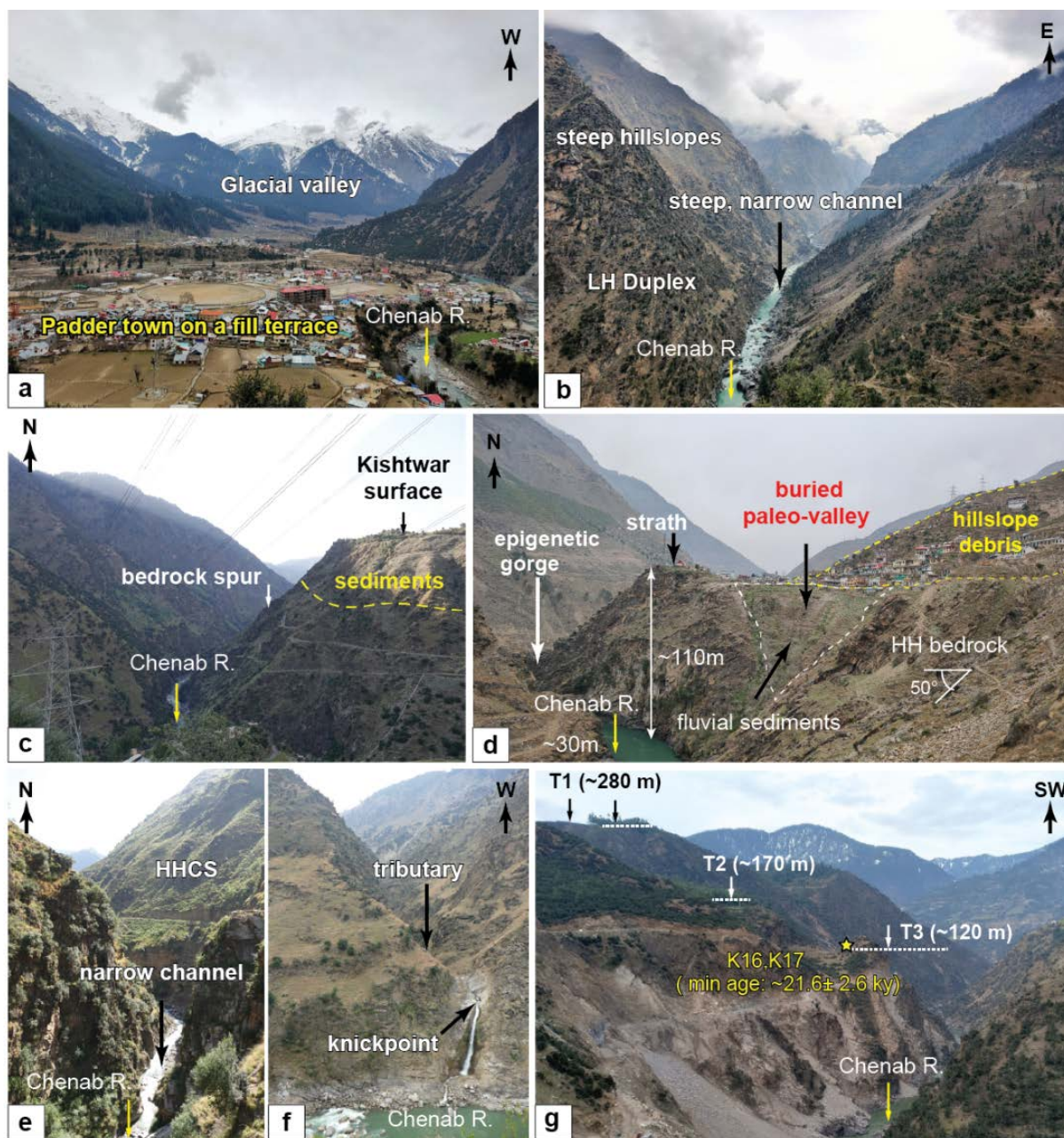
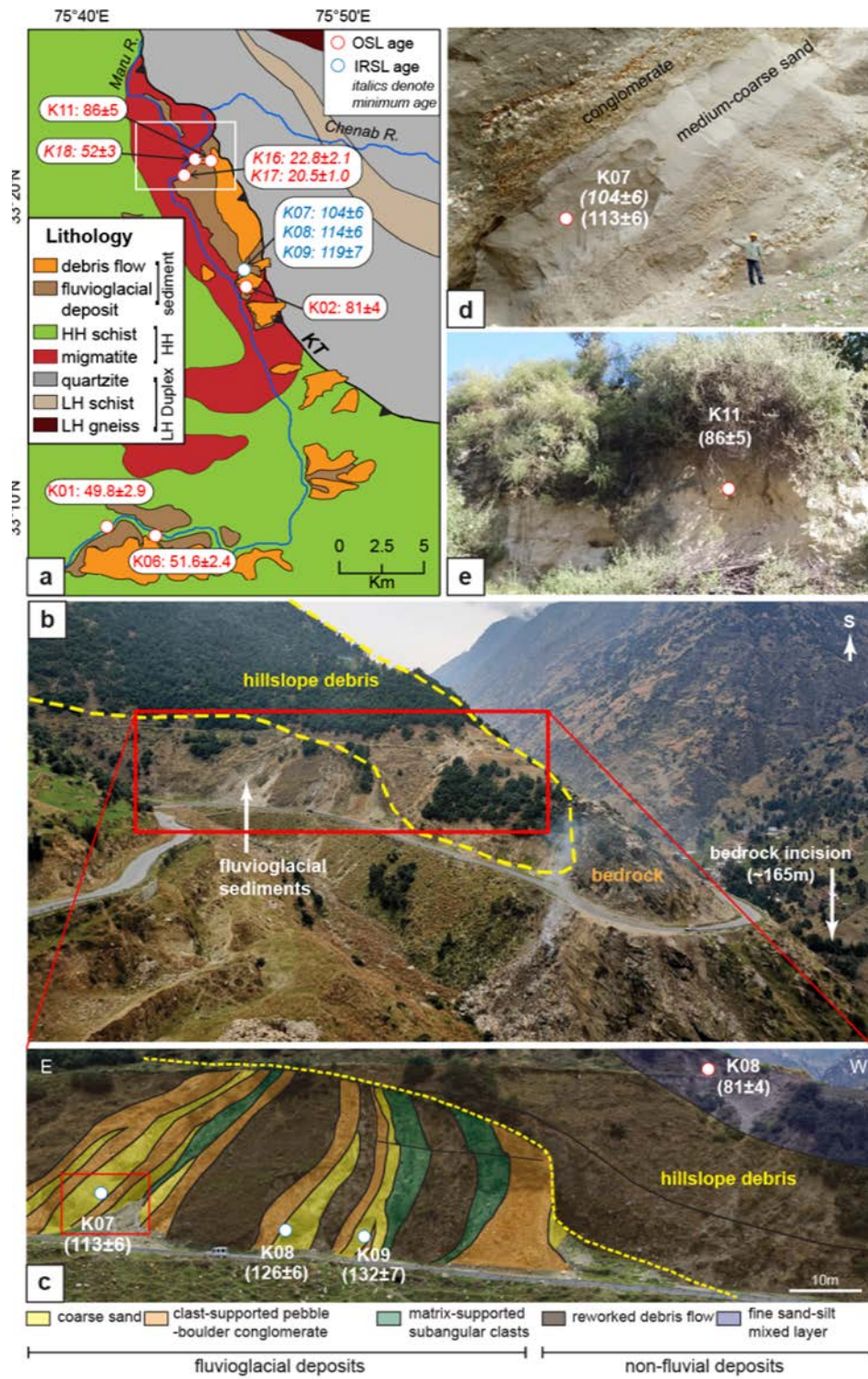
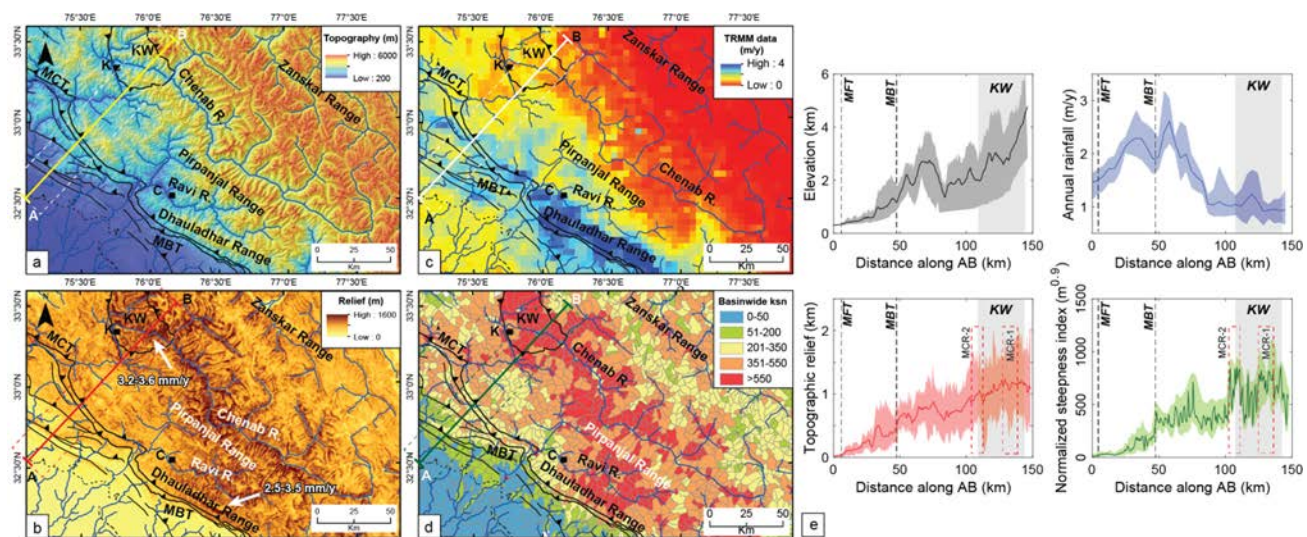


Figure 4



1209

Figure 5

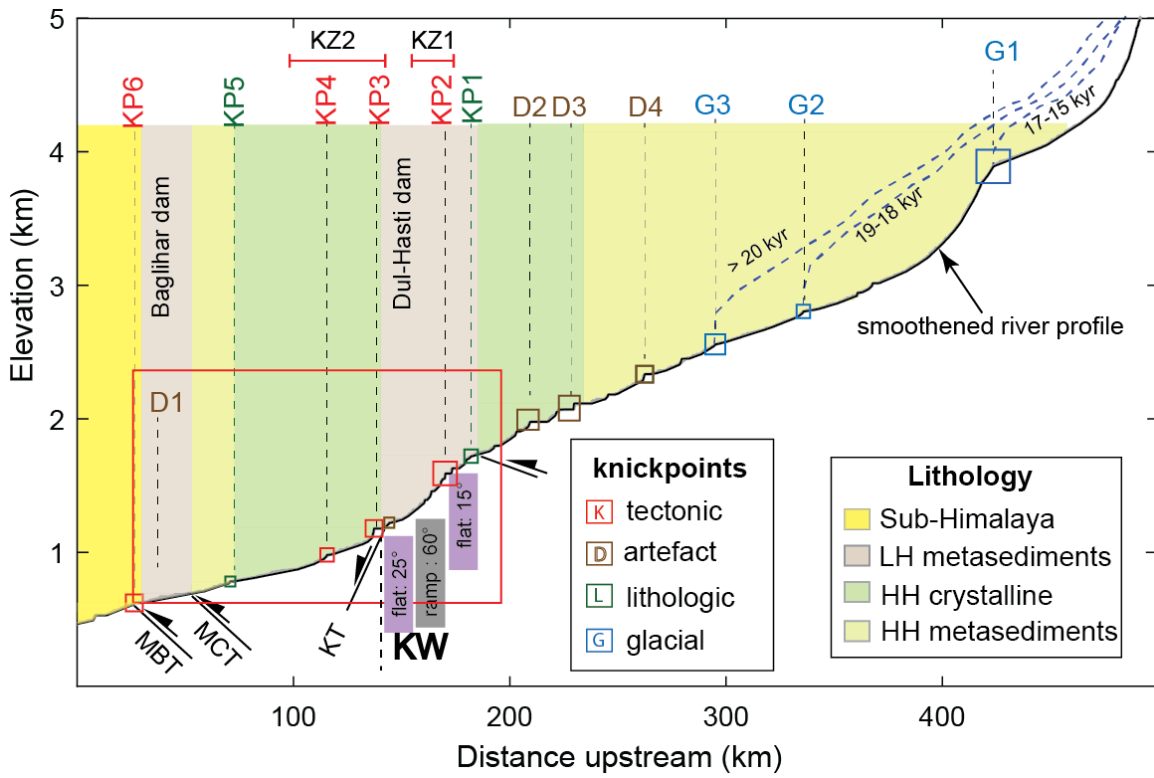


1210

1211

1212

Figure 6



1213

1214

Figure 7

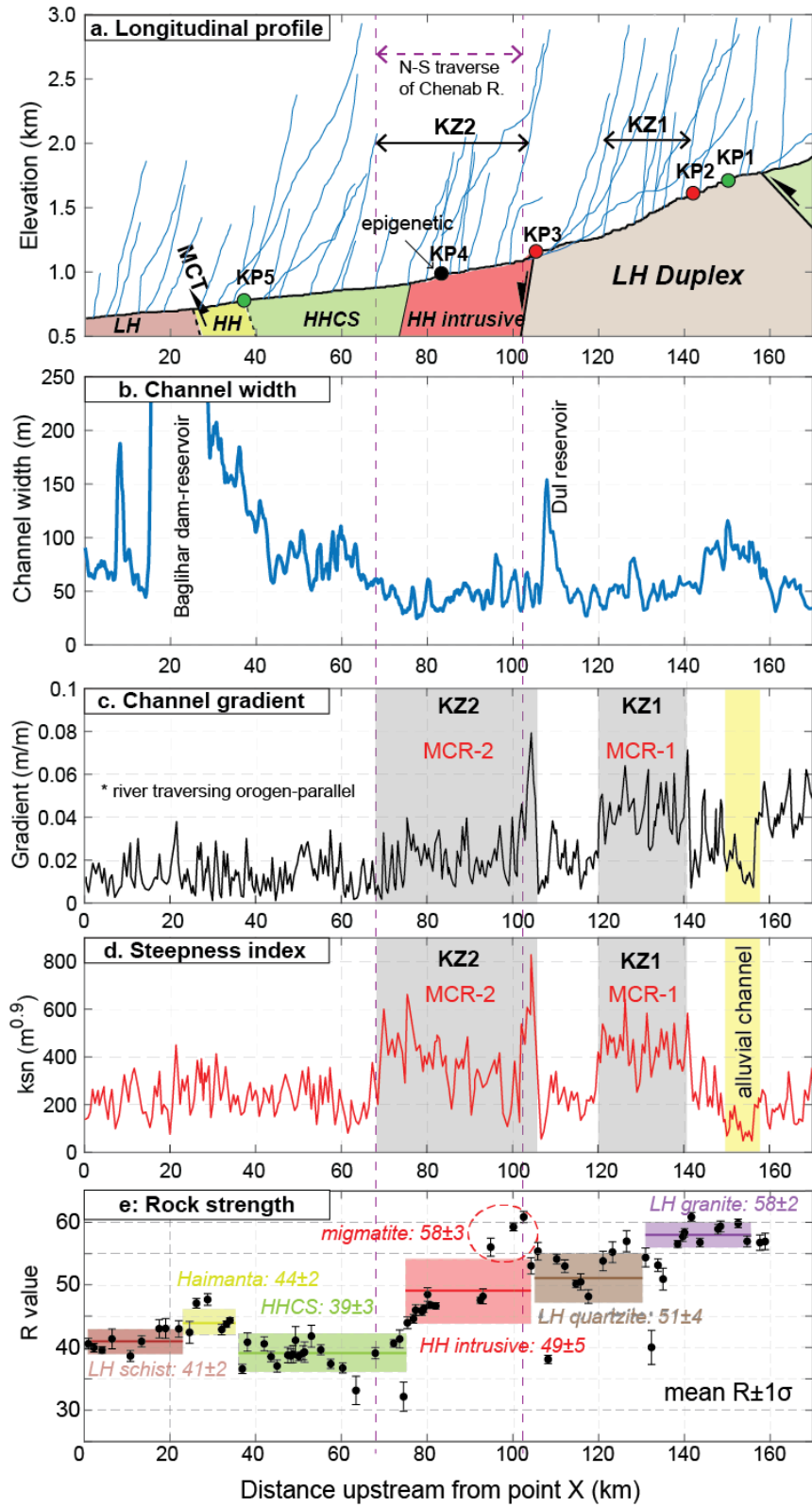
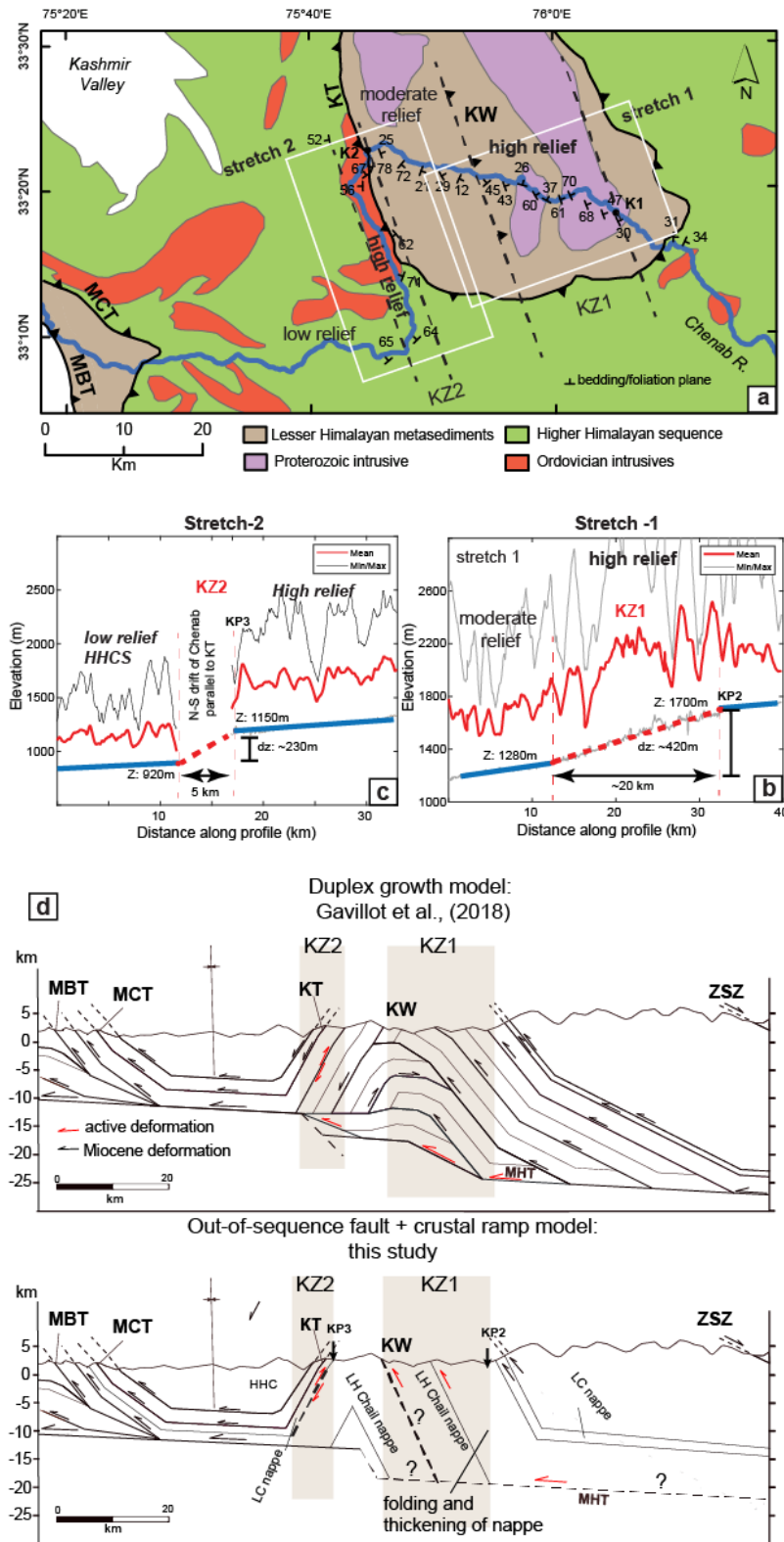
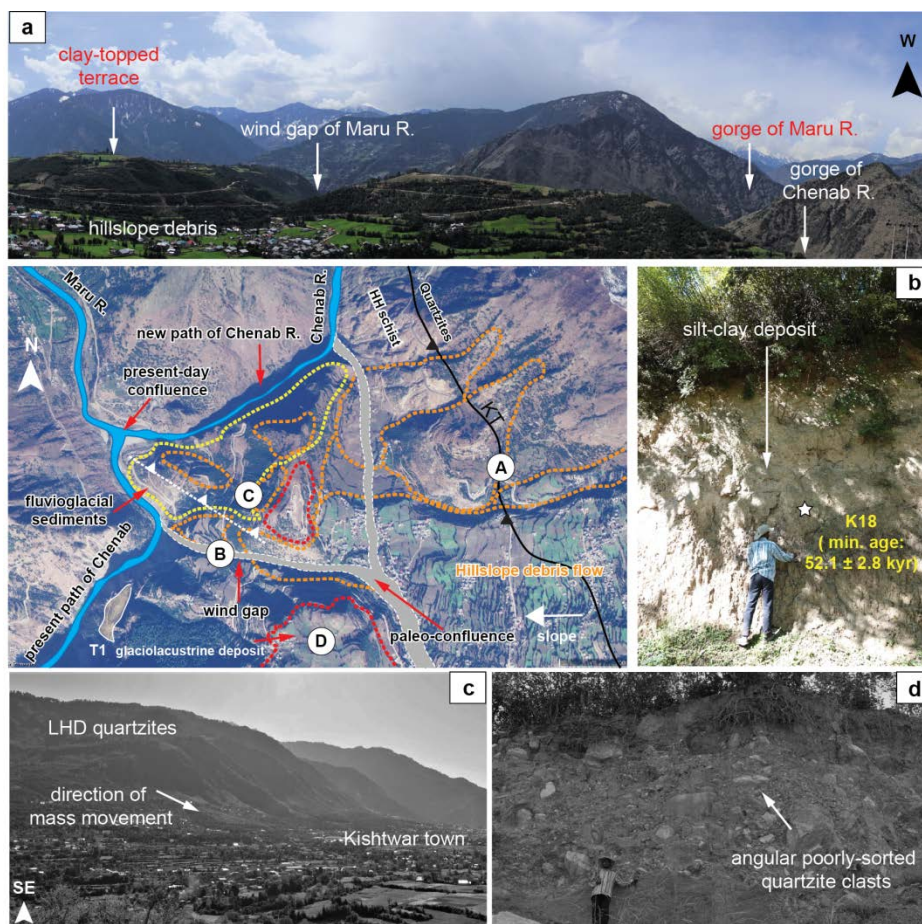


Figure 8



1221

Figure 9

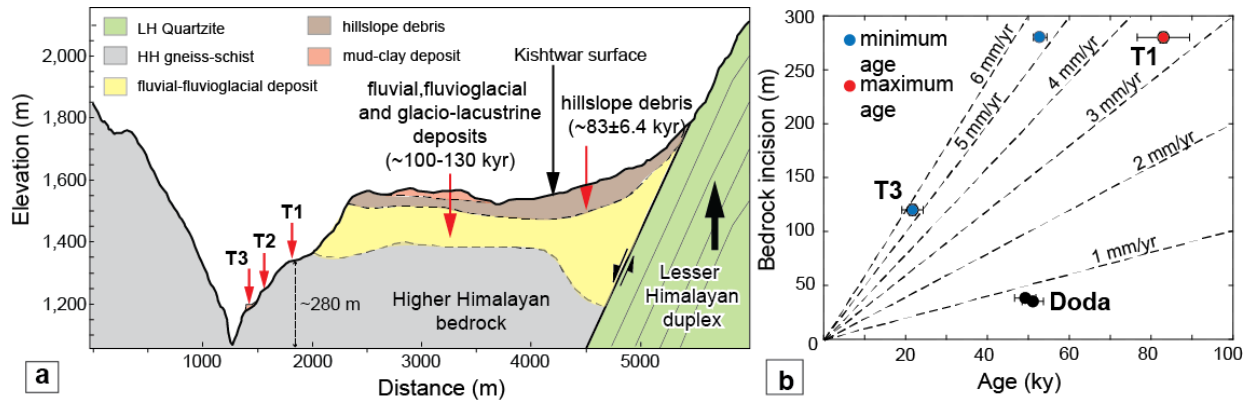


1222

1223

1224

Figure 10



1225

1226

1227

Table 1

<b>Parameter</b>	<b>downstream</b>	<b>KZ1</b>	<b>% change</b>	<b>ratio KZ1:downstream</b>	<b>downstream</b>	<b>KZ2</b>	<b>% change</b>	<b>ratio KZ2:downstream</b>
average channel gradient (m/m)	0.006	0.021	250	3.5	0.01	0.046	360	4.6
average channel width (m)	70	45	-35.7 1	0.6	55	42	-24	0.76
*Specific stream power (SSP)	0.000086	0.000467	444.44	5.4	0.000182	0.001095	502	6.02
* SSP calculated by assuming equal-discharge (Q)								

1228

1229

1230

Table 2

Sample type	Sample name	Lat (°)	Long (°)	U (ppm)	Th (ppm)	K (%)	water (%)	Dose rate (Gy/ky)	De (Gy)	OD (%)	Age (ky)	fading correction	Corrected age (ky)
<b>using central age model</b>													
OSL	K02	33.29607	75.77619	3.8	7.2	0.46	6.1	1.74±0.02	141±8	19.5	81.1±4.6		
OSL	K11	33.35352	75.74649	3.1	12.7	2.41	6	3.97±0.09	341±19	16.8	85.7±5.1		
OSL	K01	33.15222	75.66323	2.9	13.2	2.03	9	3.88±0.04	193±11	22.1	49.8±2.9		
OSL	K06	33.15243	75.70609	3.4	18	2.17	5.4	3.97±0.05	205±10	14.4	51.6±2.4		
IRSL	K07	33.2778	75.76922	3.3	13.8	2.31	5.3	4.67±0.22	489±29	16.8	104.5±5.9	0.89	113±6
IRSL	K08	33.2778	75.76922	3.5	16.9	1.97	5.6	4.61±0.23	528±38	20.5	114.4±6.3		
IRSL	K09	33.2778	75.76922	3.3	12.2	1.98	4.8	4.29±0.20	510±42	18.1	119.2±6.8	1.11	132±7
<b>using minimum age model</b>													
OSL	K16	33.34873	75.73324	3.5	16.8	2.03	7.5	3.95±0.1	90±8	40	22.8±2.1		
OSL	K17	33.34873	75.73324	3.4	18	2.17	10.5	3.96±0.11	81±3.5	46	20.5±1.0		
<b>saturated sample</b>													
OSL	K18	33.35176	75.74325	3.3	18.7	2.61	4.5	4.36±0.13	227±14		52.1±2.8		

1231

1232

1233